NTNU – Trondheim
Norwegian University of
Science and Technology

Numerical modelling of ice induced vibrations of lock-in type

Eivind Sinding-Larsen

Civil and Environmental Engineering (2 year)
Submission date: June 2014
Supervisor: Ole Andre Øiseth, KT

Norwegian University of Science and Technology
Department of Structural Engineering

Abstract

Structures located in ice infested waters are subjected to actions from moving ice. Forces are generated when a drifting ice crushes against the structure. Under certain circumstances, crushing of an ice sheet can adapt to the frequency of the structure's waterline displacement. This phenomenon is known as frequency lock-in crushing (FLC), and results in a resonant response of the structure.

An 80 seconds long interval of particularly heavy vibrations was recorded at 12:25 the 30th of March 2003 on the Norströmsgrund lighthouse. Accelerometer and force measurements from this event have been evaluated. Analyzing the event verifies that it contains frequency lock-in like characteristics. The displacement is sinusoidal and the acceleration auto spectrum confirms that the response is dominated by the first natural mode of the structure at about 2.2Hz. Comparing the displacement and force auto spectrum shows that they have similar frequency content. This is reasonable, as the ice sheet is in contact with the structure.

By integrating the acceleration signal it was made an estimate of the relative velocity between the ice and the structure. For each loading cycle it was observed that the relative velocity was low during the load build up for then to increase when the ice failed. Load measurements showed that the horizontal load distribution was concentrated to the middle of the structure when the vibrations were initiated. As the vibrations carried on, the forces in the middle gradually decreased while forces further out to each side increased slightly. For the average load, a cosine distribution is a reasonable assumption.

It has been developed a finite element program for calculating the dynamic structural response when an ice sheet impinges a structure. The finite element program was employed to simulate the recorded vibration event from Norströmsgrund 30th March 2003. First eigenfrequency of the finite element model was at 2.79Hz and the applied loading at 2.17Hz excited primarily the first mode of the structure. The numerical modelling resulted in force and acceleration signal similar to full-scale measurement, but the displacement signal was not as harmonic as in full-scale.

A numerical modelling of self-exciting vibrations due to negative damping effects was attempted with the finite element program. By tuning the formulae for stress rate in the ice, increased negative damping contribution was achieved. The response showed growing amplitudes for a period, before stabilizing at a steady state.

Sammendrag

I kalde farvann hvor sjø-is inntreffer vil drivende is som knuses mot en fastholdt konstruksjon skape store krefter mellom konstruksjonen og isdekket. Under enkelte forhold kan knusingen av isdekket tilpasse seg frekvensen til konstruksjonens forskyvning. Dette fenomenet kalles frequency lock-in crushing (FLC) og resulterer i en resonante svingninger i konstruksjonen.

Klokken 12:25 den 30. mars 2003 ble et 80 sekunder langt intervall med svært kraftige vibrasjoner målt på fyrtårnet Norströmsgrund. Aksellerometer- og kraft-målinger fra denne hendelsen har blitt evaluert. Analysen av intervallet bekrefter at var frecuency lock-in crushing som inntraff. Forskyvningssignalet var sinusformet og akselerasjons-signalets auto-spekter indikerer at svingningene primært besto av konstruksjonens første svingemode med en frekvens på ca. 2.2Hz. En sammenligning av auto-spektrene til forskyvning og kontaktkraft mellom is og konstruksjon viser at de to signalene har lignende frekvensinnhold.

Ved å integrere akselerasjons-signalet har et estimat av den relative hastigheten mellom is og konstruksjon blitt laget. For hver svinge-syklus ble det observert at den relative hastigheten var lav under lastoppbyggingen, for så å øke når isen knuste. Lastmålinger viste at den horisontale kraftfordelingen over fyrtårnets omkrets var konsentrert mot midten av kontaktflaten i det vibrasjonene bli initiert. Etter hvert som vibrasjonene pågikk ble kreftene mot midten redusert imens kreftene lenger ut på hver side økte noe. I gjennomsnitt viste en cosinus-fordeling å være representabel for lastfordelingen.

Det har blitt utviklet et elementmetodeprogram for å beregne den dynamiske responsen som oppstår når et is-dekke knuses mot en konstruksjon. Elementmetodeprogrammet ble benyttet til å simulere intervallet med vibrasjoner målt 30. mars 2003 på Norströmsgrund. Første egenfrekvens til elementmodellen var på 2.79Hz. Lasten hadde en frekvens på 2.17Hz og den eksiterte i hovedsak første svingemode. Elementanalysen resulterte i last- og akselleraSjons-signal som tilsvarte full-skala målingene. Forskyvningssignalet fra analysen var ikke fullt så harmonisk som forskyvningene i full-skala.

Det ble i tillegg utført en analyse, der dynamisk respons som et resultat av negativ demping ble forsøkt oppnådd med elementmetodeprogrammet. Ved å tilpasse formlene for spenningsrate ble effekten av negativ demping økt. Resultatet var en dynamisk respons som vise økende amplitude før den stabiliserte seg på et stabilt nivå

Preface

This thesis was written at the Department of Structural Engineering during the final semester of the study program Civil and Environmental Engineering at the Norwegian University of Science and Technology. The author has previously achieved a Bachelor's degree in Civil Engineering from the University of Agder. During the master's degree study, he has specialized within the finite element method and structural dynamics.

The working process has been challenging but also rewarding. The task required a solid study in the available literature on ice mechanics and ice induced vibrations, before any production of useful results could begin. During the process, valuable experience with utilization of published technical literature has been gained. The author has also attained new skills in computer programming. He found it rewarding to be able to apply inherent competence in structural dynamics on a new kind of issue.

The author would like to thank Morten Bjerkås from REINERTSEN AS for his sharing of knowledge on the subject of ice induced vibrations. Several interesting meetings and discussions have certainly increased my interest on the subject. Supervisor at the Department of Structural Engineering, Ole Øiseth has shown a positive attitude and support in courses and projects during my time at NTNU. My interest in structural dynamics is largely thanks to him. Finally, co-supervisor Torodd Nord has showed great interest in the thesis and contributed with several ideas and suggestions.

Eivind Sinding-Larsen

Trondheim, 10.06.2014

Contents

Notation

Roman letters:

A = Area of interaction zone
A_0 = Reference area
$[\mathbf{C}]$ = Damping matrix
C = Damping constant
c = Ice crushing length
d = Width of contact area
E = Young's modulus
F = Force
F_D = Damping force
F_{ext} = Externally applied force
F_G = Global ice load
F_I = Inertia force
F_S = Stiffness force
F^T = Tangential force
f = Frequency (Hz)
H = Frequency response function
h = Ice thickness
I = Second moment of area
K_{eff} = Effective stiffess of ice sheet
l = Element length
$[\mathbf{K}]$ = Stiffness matrix
K = Stiffness constant
$[\mathbf{M}]$ = Mass matrix
M = Mass constant
N = Increment counter
n = Ratio between inner and outer radius
p = Pressure
q = Radius of gyration
r = Radius
S_x = Auto spectral density of variable x
t = Time
u = Displacement of structure
$[\mathbf{u}]$ = Response vector
v_{ice} = Ice velocity
v_{rel} = Relative velocity between ice and structure
X = Fourier component
x = Arbitrary signal
z = Loading length

Greek letters:

α_0 = Rayleigh damping coefficient
α_1 = Rayleigh damping coefficient
β = Newmark method coefficient
δ = Deformation in ice sheet
ε = Strain
Φ = Shear factor
φ = Scaling factor
γ = Newmark method coefficient
κ = Shear coefficient
μ = Friction coefficient
ν = Poisson's ratio
θ = Angle off ice drift direction
ρ = Mass density
σ = Stress
σ_C = Ice crushig capacity
ω = Frequency (rad/s)
ζ = Damping coefficient

1 Introduction

This work is aimed to contribute to knowledge on numerical modelling of dynamic response for fixed offshore structures subjected to ice loads. In the thesis, an event of severe vibrations on the Norströmsgrund lighthouse is evaluated. A finite element program, developed to simulate this event, will be presented. This introductory chapter presents the concepts of ice induces vibration and frequency lock-in crushing. A short recapitulation of previous research on the topic is given. The regarded structure, the Norströmsgrund lighthouse, and the vibration event are presented in detail. Finally, the scope of the work is addressed.

1.1 Background

For bottom fixed structures located in ice-infested waters, dynamic loading from drifting pack ice may lead to unwanted ice-induced vibrations (IIV). During crushing of ice against a compliant structure, the contact force will to begin with gradually increase when the structure resists movement of the ice sheet. At this point, both ice and structure are under elastic deformation, and strain energy is stored. At one point, the crushing capacity of the ice is reached, and it collapses. This results in a sudden decrease in contact force, and the structure swings back as strain energy is released. Ice velocity and crushing length will determine how soon a new loading sequence will commence.

In general, crushing characteristics during IIV can be categorized into three regimes, as shown in Fig. 1.1. At low ice velocity, intermittent crushing of the ice occurs. The response is then quasi-static during the load build up, resulting in a saw tooth like force time history and response. At high ice velocity the crushing is continuous and occurs with a random stationary response. Within both intermittent crushing and continuous crushing, frequency lock-in crushing (FLC) may occur. Frequency lock-in means that the ice force frequency attains the natural frequency of the structure, even under variations in ice conditions (Yue et al., 2009). During FLC, the response reaches steady state. The accelerations during FLC are far greater than during intermittent and continuous crushing, because the vibrations become resonant.

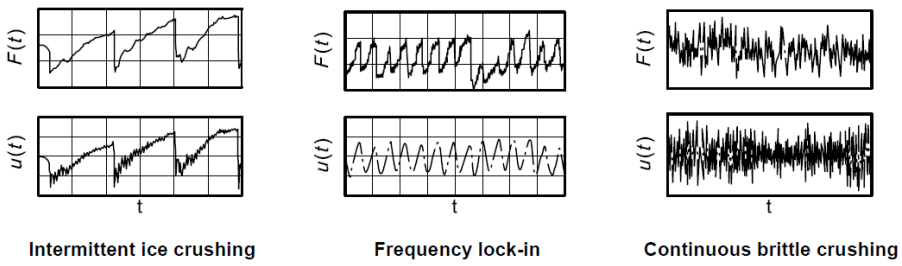

Figure 1.1 Ice crushing regimes (ISO, 2010).

The crushing capacity of ice σ_C is dependent on the strain rate $\dot{\varepsilon}$, shown in Fig. 1.2. At low ice velocity the failure of the ice is in the ductile domain, while during high ice velocity it is primarily in the brittle domain. Because frequency lock-in occurs at ice velocities higher than at intermittent crushing and lower than at continuous crushing, it is commonly believed that the ice behavior is in the transitional domain in this vibration mode (Kärnä and Turunen, 1989).

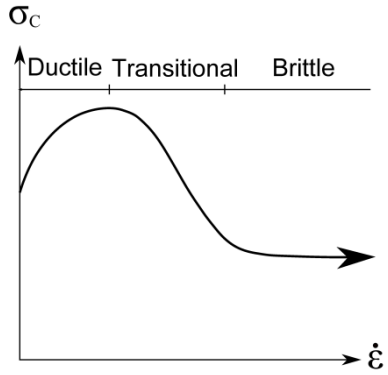

Figure 1.2 Strain rate dependency of crushing strength.

Crushing of ice in front of a structure is not always simultaneous over the interaction area. Radial cracks, illustrated in Fig. 1.3, divide the ice sheet into separate contact zones (Palmer et al., 1983). Synchronization between crushing in the different contact zones is of significance for the magnitude of the global load. Both full-scale and laboratory tests indicate that the crushing has a tendency to synchronize during FLC, while it is non-synchronized during continuous brittle crushing (Bjerkås, 2006, Kärnä et al., 1999). Naturally the peaks of the global load will be greater when failure in the crushing zones is synchronized.

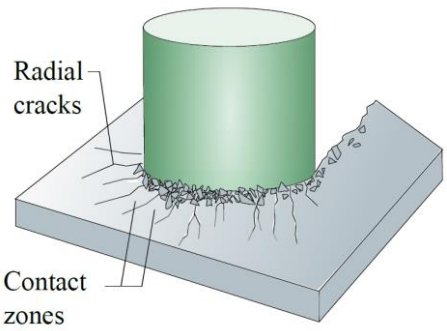

Figure 1.3 Contact zones in ice structure interaction.

If the occurrence of IIV are frequent, they may lead to fatigue issues. In addition, vibrations of higher amplitude can produce accelerations affecting the serviceability of the structure. For flexible structures FLC can excite fluctuations in one or more of its natural modes (Sodhi, 1988). In the ultimate case resonant vibrations from FLC can lead to structural failure, as dynamic amplification

produces displacements several times larger than those from a static deformation (Kärnä, 1992). Lock-in like resonant vibrations caused by dynamic ice forces stem from a complicated ice structure interaction. Because the effect can cause harm to the structure, it is desirable to better understand the phenomenon. Even though FLC is a seldom occurrence instance it has led to collapse for several structures. It is therefore an important event to address.

1.2 History of research on IIV

A brief summary of some important publications regarding FLC is given.

In a his doctoral thesis, Peyton (1968) documented field measurements of contact force between drifting sea ice and a vertical test pile erected on a temporary drilling platform in Cook Inlet, Alaska. These recordings were some of the first to document the phenomenon of lock-in like ice induced vibrations. Peyton observed that the ice force was greatest when the ice failure was of a slow ratcheting nature. He also noticed that the force magnitude fluctuated at a rate approximate to the structure's resonant frequency, but attributed this to be a coincidence. Peyton described the rate dependency of ice crushing strength, and presented a curve for the ice crushing strength as a function of stress rate.

Matlock et al. (1969) presented a theoretical model for ice structure interaction. The model consists of a series of elastic-brittle element that impinge on a single degree of freedom system. Matlock's model was able to describe low amplitude high frequency vibrations about a mean value at high ice velocity, as well as high amplitude vibrations at low ice velocities. However, the model did not incorporate any ice properties, but employed a loading believed to simulate that of true ice.

Blenkarn (1970) presented a paper on results from ice force recordings on offshore structures in Cook Inlet, Alaska. By the means of strain gauges, load cells and accelerometers, the force variations and structural vibrations could be documented. Just as Peyton, Blenkarn observed severe vibrations of the regarded structures. Ice was known to show decreasing strength at increasing stress rates. Blenkarn stated this would result in negative damping, leading to *self-exciting* vibrations. He attributed the self-exciting vibration mechanism to "…almost certainly play an important part in much of the dynamic behavior observed in Cook Inlet structures".

Michel and Toussaint (1977) proposed a division of ice failure mode at different strain rates. They described the ice crushing behavior as being in either the *ductile* zone, *transition* zone or *brittle* zone.

Määttänen (1978) proposed a mathematical model for describing self-exciting ice-induced vibrations. By combining the equations of motion for the structure and the average rate dependent ice crushing strength, he established an autonomous set of equations. The equation set made the ice and the structure form a closed loop system, where each affected another. The model was used to predict the occurrence of self-excitation.

Sodhi has in several publications stated that IIV is a form of *forced vibrations* and cannot be self-exited due to negative damping (1988, 1991). The definition of self-excitation given by Den Hartog (1956), states that during pure self-excitation the excitation force should vanish when the system is prevented from moving. This would not be the case for an ice sheet crushing against a structure which is being held still. Forced vibrations indicate that the frequency of ice failure is due to ice properties, and not governed by the natural frequency of the structure.

The frequency of vortex shedding from wind on a cylindrical object can be predicted by the Strouhal number. Sodhi suggested that analogue the Strouhal number describing the frequency of vortex induced vibrations, the frequency of ice force can be described by the relation fh/v_{ice} , where $f =$ crushing frequency, $h =$ ice thickness and $v_{ice} =$ ice velocity. A characteristic crushing length will dictate the crushing frequency.

Kärnä has presented several numerical models for ice structure interaction. His methods imply dividing the ice sheet, the structure and the soil into separate substructures (Kärnä, 1992). The ice sheet is divided into a body named far field and a body named near field. Ice mechanical crushing features are given to the near field zone. Both near field and far field are further divided into zones, giving possibility for non-simultaneous crushing over the contact surface.

The International Organization for Standardization has produced a code that includes a procedure for determining the design load for structures subject to ice induced vibrations (ISO, 2010). The method consists of applying a saw-tooth shaped load, with prescribed period equal to the first natural period of the structure. The magnitude of the peak load is defined as a function of expected ice thickness, structure width and ice strength. The fact that the load is predefined makes the calculated response a form of forced vibration.

1.3 The Norströmsgrund lighthouse

Norströmsgrund lighthouse was deployed in 1971 in the gulf of Botnia, about 60km south east of Luleå (Bjerkås, 2006). In Fig. 1.4 the geometry is illustrated. The structure is a concrete tower fixed to a concrete caisson of 23m in diameter. The caisson is resting on dense sand at a water depth of

14.15m at mean water level. Sand is used as ballast in the caisson and the lower part of the tower. To ensure a stable foundation, the seabed under the caisson is leveled with crushed stone stabilized by cement grout (Björk, 1981). Total height of the structure is 42.35m above seabed.

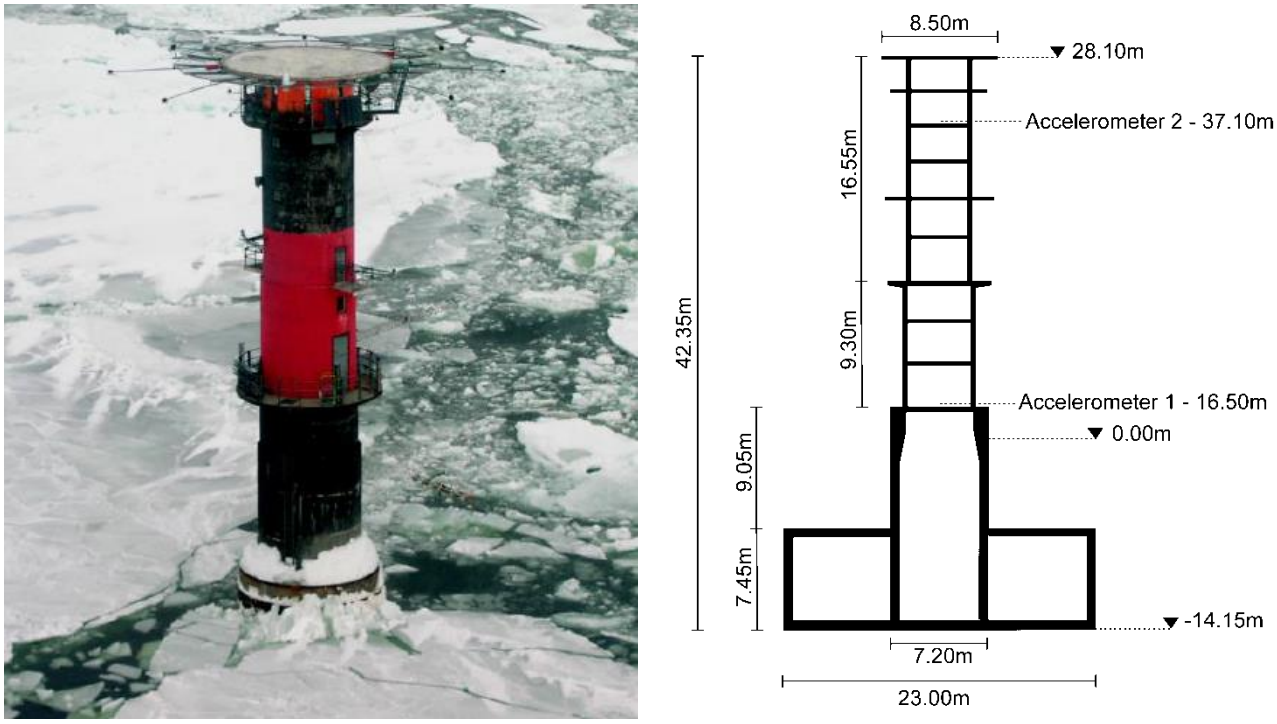

(a) (b)

Figure 1.4 (a) Norströmsgrund lighthouse (Kärnä and Yan, 2003). (b) Structure geometry.

Regarding IIV, Norströmsgrund is one of the most studied structures there is. As early as during the winter of 1971-72, service staff observed heavy oscillations as the tower cut through drifting ice. Maximum accelerations of 0.1g and vibrations at a frequency of about 2.8Hz were recorded in the end of this first winter in the structure's lifetime. Since then, several research programs have evolved around the IIV of this particular structure.

In 1999 an industry-EU collaboration research project called "LOw LEvel Ice Forces" (LOLEIF) began measurements on the structure. Nine load panels, shown in Fig.1.5, were mounted on the structure, covering almost half the waterline circumference. In the period from 2001 to 2003, inclinometers and accelerometers were included to the data collecting. Video recordings, a laser device, a sonar device and an electro-magnetic device recorded ice thickness and velocity. In 2001 the project "Measurements on STRuctures in ICE" (STRICE) was started. STRICE continued the measurements done under LOLEIF for three more years (Bjerkås, 2006).

Figure 1.5 Force panels at Norströmsgrund (Bjerkås, 2014).

1.4 The 30031225 FLC-event

An event of exceptionally heavy vibrations occurred at Norströmsgrund 12:25 the 30th March 2003. From now on this particular event will be referred to as the 30031225 FLC-event. Recordings made under the STRICE project captured details on forces and accelerations. A detailed description of the event is given in a publication by Bjerkås, Meese and Alsos (2013). Ice velocity during the event was measured to 0.065m/s while ice thickness was 0.70m. The sampling frequency of the accelerometers were 84Hz. Video recordings reveal that during crushing of drifting ice against the lighthouse, ice rubble piled up in front of the structure. At one point the weight of the rubble, combined with the compressive forces on the ice edge, caused the ice sheet to collapse. This failure resulted in a circumferential crack in the ice sheet, some length in front of the structure. The failure was similar to what Kärnä and Jochmann (2003) denotes as a *one-hinge bending failure*. In Fig. 1.5 snapshots from the video recordings illustrate the crack approaching the lighthouse.

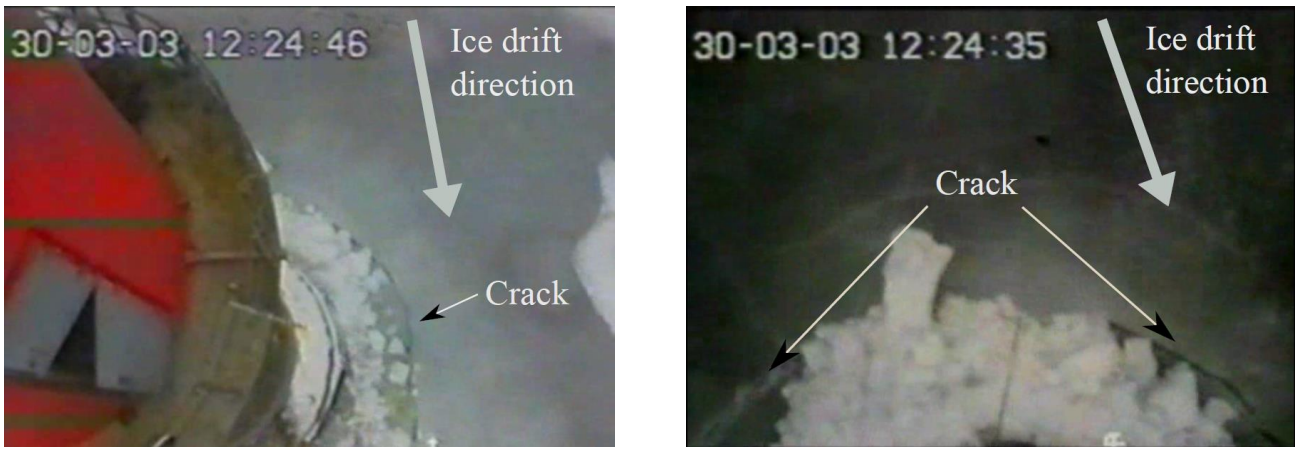

Figure 1.5 Semicircular crack approaching lighthouse.

After this bending failure, the ice sheet was weakened and ice forces on the structure were low. The FLC event is pointed out in Fig. 1.6. Fig. 1.7 shows how the ice force started to gradually increase as the intact ice sheet gained contact with the structure at 12:25:30.

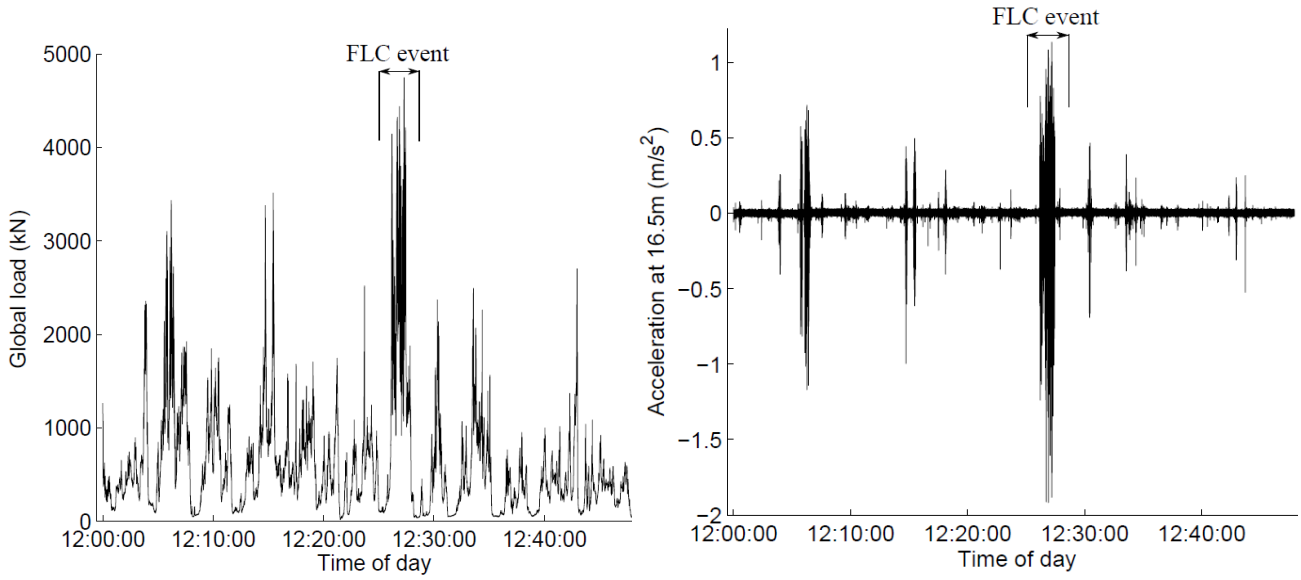

(a) (b)

Figure 1.6 (a) Global load measured 30th of March 2003. (b) Acceleration measured 30th of March 2003.

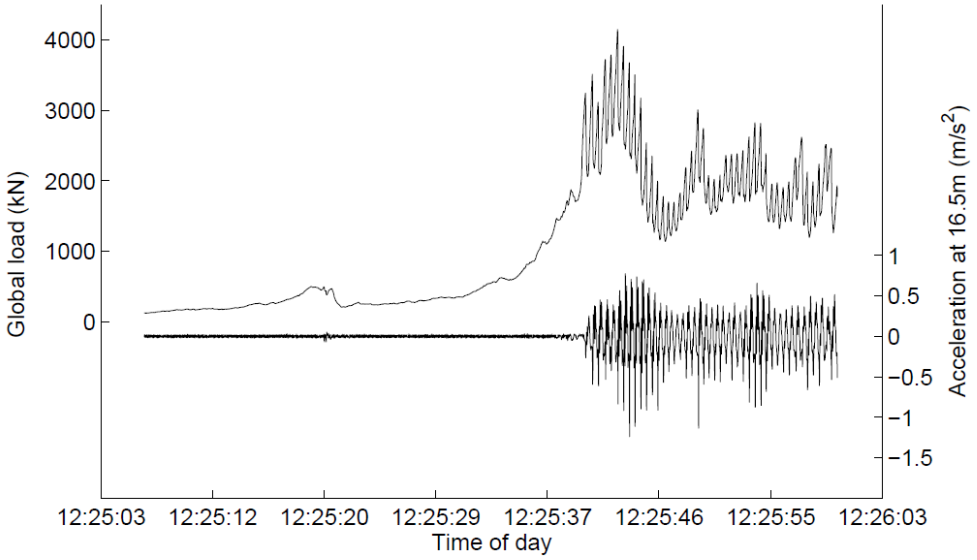

Figure 1.7. Onset of forces and accelerations during lock-in event the 30th March 2003.

1.5 Scope of work

In this thesis a numerical calculation tool for determining the structural response during FLC is presented. The model includes the rate-dependent properties of ice and implements ice contact in several discrete contact points. The tool will be benchmark tested against data from full-scale measurement made during the 30031225 FLC-event at the Norströmsgrund lighthouse.

2 Method

This chapter will give insight into how data from force and accelerometer measurements is processed and utilized in order to assess the dynamic response of the lighthouse. The chapter also presents the theory behind the finite element program developed for simulating the vibration event on Norströmsgrund. Finally the structure of the finite element program itself is presented.

2.1 Calculation of global load

The ice loads working on the Norströmsgrund lighthouse were measured with nine load panels as presented in Fig 2.1(a). Each load panel measured the compressive force in the radial direction. However, the data from the load measurements are not sufficient to directly establish the global load affecting the lighthouse. First of all, the load panels do not measure contributions from tangential friction shear forces between the ice and the structure. Fig. 2.1(b) illustrates this. Secondly, the load panels extend over about 162˚ of the perimeter, so the load panels will never cover the entire interaction area. Due to these deficiencies, some assumptions have to be made in order to estimate the magnitude of the global load.

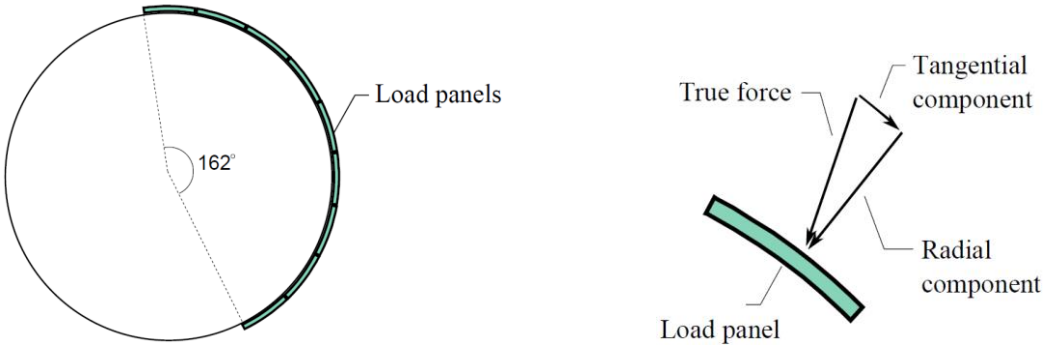

(a) (b)

Figure 2.1(a) Load panel on Norströmsgrund. (b) Radial and tangential component of force on load panel.

In the literature it is a bit unclear how much of the circumference the load panels cover. According to Kärnä and Yan (2003) the load panels cover 144˚, Jochmann (2003) says 162˚ while Bjerkås (2006) states 167˚. In this work it is assumed that each of the nine panels cover 18˚, making a total of 162˚. In addition it is assumed that the center of the first panel is oriented directly towards north. Each panel is named after their orientation, starting at panel P0 which is oriented at 0˚. This is illustrated in Fig. 2.2.

2.1.1 Force direction

The direction of the structural response gives an indication of the direction of the integrated global load acting on the structure. A scatterplot of the displacement peaks during the first minute of the

30031225 FLC-event is shown in Fig. 2.3. The displacements indicate that the average direction of the force is from 45˚. When calculating the global load based on the force panel measurements, each panel's contribution will be the panel force's component in this direction.

The sign convention used in all calculation is based on that compressive ice forces are denoted positive and that a positive force results in a positive displacement.

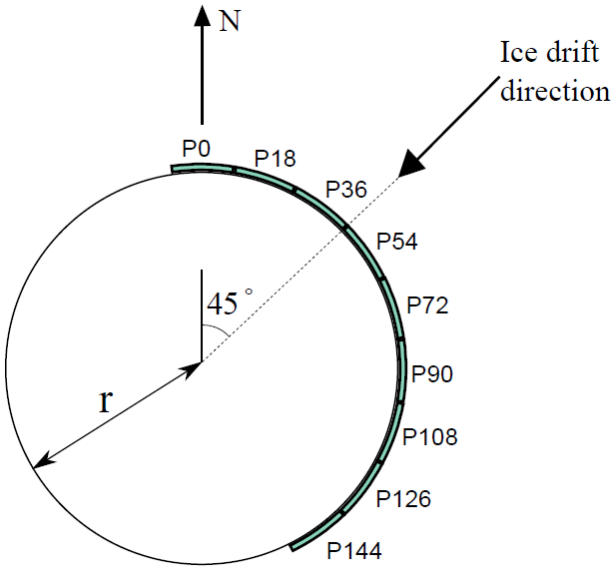

Figure 2.2 Force panel setup.

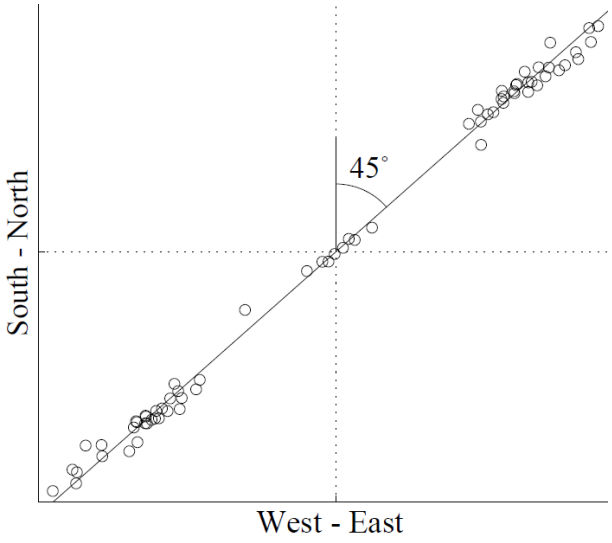

Figure 2.3 Direction of displacements during 30031225 FLC-event.

2.1.2 Contribution from friction shear forces

When measuring the contact force between ice and a structure, the measurements are normally limited to normal loads. Calculation of global load is also most often done by only including contribution from normal forces. This is a simplification, as friction shear forces acting tangential to the surface of the structure will contribute to deflecting it. In 1987, three biaxial load panels were installed on Norströmsgrund, by the Hamburg Ship Model Basin. These panels were able to measure both normal forces and tangential forces (Wessels et al., 1989). Fig. 2.4 shows the force panel setup. Results from these measurements give some indication on the magnitudes of shear forces present during IIV.

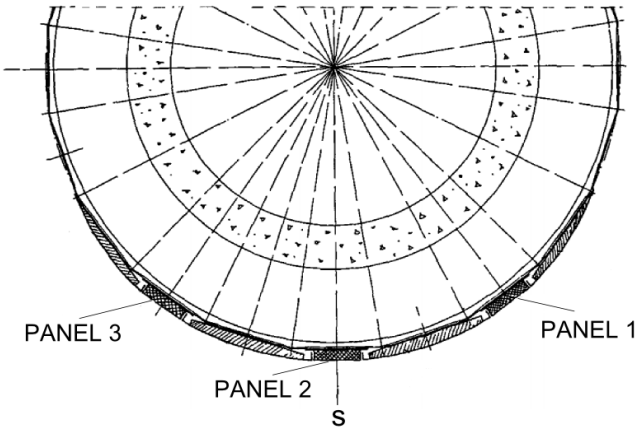

Figure 2.4 Force panel set up during biaxial force panel measurements (Wessels et al., 1989).

Assuming Coulomb friction, the friction coefficient μ is defined as the ratio between tangential component and normal component from a force on a surface. An estimation to the friction coefficient during ice structure interaction is made by calculating the ratio between tangential and normal load measured by Wessels et al.(1989). The results are presented in Table 2.1. In average, the friction coefficient is about 0.2.

Panel number	**Average tangential load (kN)**	**Average normal load (kN)**	μ
1	9.0	40.5	0.22
2	9.5	45.1	0.21
3	17.9	101.0	0.18

Table 2.1 Friction coefficient during biaxial load measurement by Wessels et al. (1989)

Frederking and Barker (2001) report an average friction coefficient between sea ice and painted steel of 0.05 for speeds greater than 0.05m/s. For corroded steel the coefficient was 0.1 for speeds greater than 0.1m/s increasing to 0.2 at 0.01m/s. The load panels mounted during LOLEIF and STRICE were of painted steel, but pictures indicate that some corrosion may have been present on these panels when the 30031225 FLC-event took place. The relative velocity between the lighthouse and the ice sheet during the event varied between 0.045 and 0.085m/s. According to Frederking and Barker the friction coefficient should hence be somewhere between 0.05 and 0.2.

Based on the biaxial force measurements by Wessels et al., and the friction coefficient measurements by Frederking and Barker, a common ground is sought by choosing a friction coefficient of 0.20 in further calculations.

Ice friction is very complex and depends on several factors such as normal force, surface roughness, temperature and relative velocity (Sukhorukov and Marchenko, 2014). By assuming a constant friction coefficient and Coulomb friction, one can, in an approximate manner, include friction shear

forces when calculating the global load. Based on the known normal forces, global load including shear force contribution can be calculated by Eq. (2.1). The formula is similar to what has been proposed by Kärnä and Yan (2003).

$$F_G = \sum_{i=0}^{126} F_i \cos(\theta_i) + F_i^T \sin(\theta_i) \tag{2.1}$$

where F_i is the measured panel force, i = panel number 0, 18, 36, 54, 72, 90, 108, 126, and $F_i^T = \mu F_i$ is the tangential friction force contribution . A principle sketch of F_i^T and F_i is illustrated in Fig. 2.5.

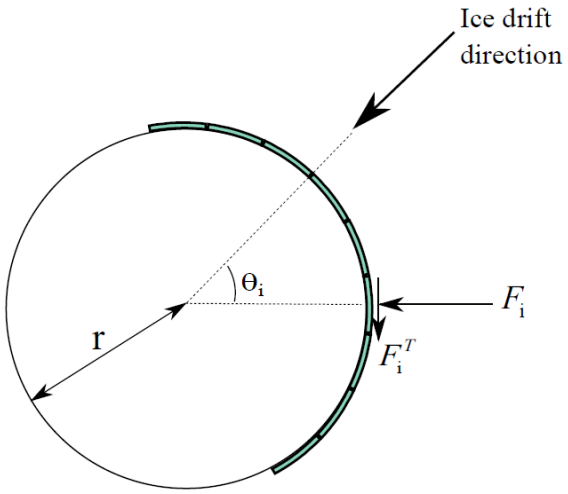

Figure 2.5 Normal and tangential force component using Coulomb model.

When calculating the global load, the friction coefficient has to be determined. Determining the friction coefficient does however come with uncertainty. By applying Eq. (2.1) on force measurements from the 30031225 FLC-event, it has been performed a parameter study that illustrates the calculated global loads sensibility to changes in friction coefficient. Fig. 2.6 shows how the calculated average global load increases with increasing friction coefficient. The relation is almost linear, and it displays that a deviation of 0.1 in friction coefficient leads to a 7% error in global load. Assuming that the friction coefficient is 0.2, neglecting friction forces gives a 14% error in calculated global load. It should be pointed out that the slope of the line in Fig. 2.6 is not general, but related to the horizontal force distribution during the particular event.

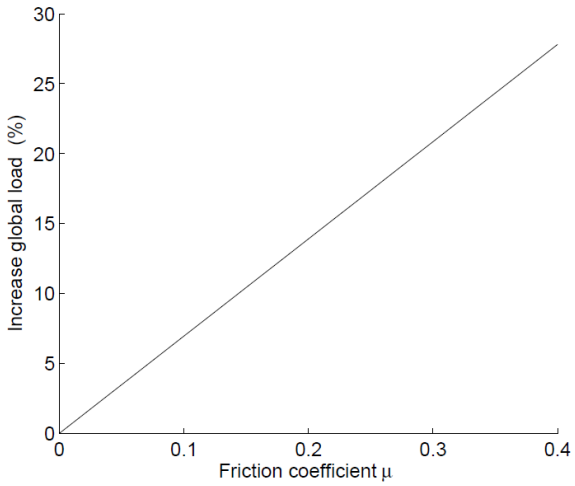

Figure 2.6 Relation between friction coefficient and increase in global load.

2.1.3 Interaction area without force panels

Because the load panels do not cover the entire perimeter of the structure, there will be areas of the interaction zone, where forces are not recorded. During the 30031225 FLC-event, the ice drift direction was from approximately 45˚. Assuming that the interaction extends in a sector of 90˚ to each side of the drift direction, it becomes clear that the load panels do not cover the entire interaction zone during this event.

Fig 2.7 shows the horizontal force distribution in the interaction zone, for every 0.2 seconds during the first 25 seconds of the frequency lock-in. Panel P0 is showing small, but not negligible, forces. It is therefore reason to believe that there are some forces acting on the structure outside of panel P0. To include the forces acting outside of the measuring panels it has been established a virtual load panel, named panel VP-18 (virtual panel at -18˚). Fig. 2.8 shows the additional panel.

Panel P0 is the third panel from the center at 45˚ and counting towards north. Looking at the relation between P108 and P126, which are the panels 3 and 4 from center counting towards south, forces on P126 is quite consistently about half of those on P108. The load on panel VP-18, is therefore at all times set to be 50% of the load on P0.

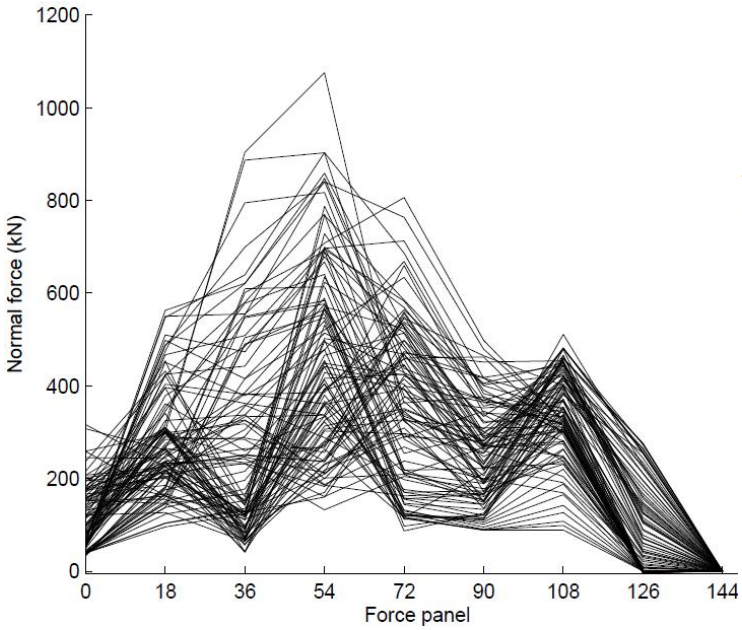

Figure 2.7 Force distributions.

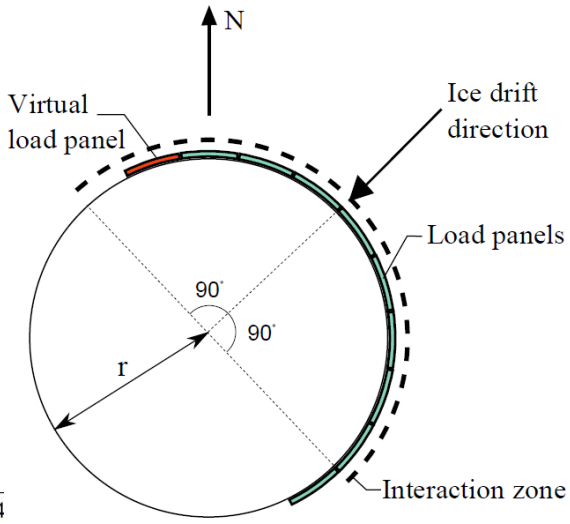

Figure 2.8 Virtual load panel.

2.2 Numerical solution of equation of motion

Numerical modelling of ice induced vibrations requires a procedure for calculating the dynamic response of a structure. The behavior of a system undergoing dynamic displacements is normally described by a differential equation, called the equation of motion, given in Eq. (2.2).

$$F_I(t)+F_D(t)+F_S(t)=F_{ext}(t) \tag{2.2}$$

where index *I* denotes inertia forces, *D* denotes damping forces, *S* denotes stiffness forces and *ext* denotes externally applied load on the system. For a multi degree of freedom system the forces can be calculated by the following expressions

$$\{\mathbf{F}_I\}=[\mathbf{M}]\{\ddot{\mathbf{u}}\} \tag{2.3}$$

$$\{\mathbf{F}_D\}=[\mathbf{C}]\{\dot{\mathbf{u}}\} \tag{2.4}$$

$$\{\mathbf{F}_S\}=[\mathbf{K}]\{\mathbf{u}\} \tag{2.5}$$

where $[\mathbf{K}]$, $[\mathbf{C}]$ and $[\mathbf{M}]$ is representing the global system stiffness, damping and mass matrix respectively. $\{\mathbf{u}\}$ is the structural response vector. The dot symbolizes time derivative, and hence give label to the structural velocity and acceleration.

2.2.1 Direct integration

During ice structure interaction, the contact force will depend on the structural response. By including ice failure in the description of contact force, a non-linearity is introduced to the system. Non-linear vibration problems can be solved by semi-analytical or numerical methods (Langen and

Sigbjörnsson, 1979). When using numerical methods, the response is normally solved by direct integration. With direct integration, the response time history is calculated in small time steps, by integrating the acceleration during the time step to get the velocity and displacement. This is done directly, without transforming the differential equations to a modal form. Therefore, the eigenvalue problem does not need to be solved. Good accuracy when using direct integration demands the time step Δt to be sufficiently small. Solution algorithms can be divided into *implicit* or *explicit* methods.

Implicit methods imply that the displacement at step $n+1$ satisfies the equation of motion at this step, giving

$$\{\mathbf{u}\}_{N+1} = f(\{\dot{\mathbf{u}}\}_{N+1}, \{\ddot{\mathbf{u}}\}_{N+1}, \{\mathbf{u}\}_N, \{\dot{\mathbf{u}}\}_N, \{\ddot{\mathbf{u}}\}_N, \ldots) \tag{2.6}$$

Explicit methods use information at step n to determine the response at step $n+1$ (Cook et al., 2002)

$$\{\mathbf{u}\}_{N+1} = f(\{\mathbf{u}\}_N, \{\dot{\mathbf{u}}\}_N, \{\ddot{\mathbf{u}}\}_N, \{\mathbf{u}\}_{N-1}, \ldots) \tag{2.7}$$

2.2.2 The Newmark method

Two common implicit direct integration methods are the *Constant Average Acceleration Method* and *Linear Acceleration Method.* The names stem from the assumptions made for the acceleration during the forthcoming time step. The following expressions represent the methods, for a single degree of freedom system.

Constant Average Acceleration Method:

$$\dot{u}_{N+1} = \dot{u}_N + \frac{1}{2}\Delta t(\ddot{u}_{N+1} + \ddot{u}_N) \tag{2.8}$$

$$u_{N+1} = u_N + \Delta t\,\dot{u}_N + \frac{1}{4}\Delta t^2(\ddot{u}_{N+1} + \ddot{u}_N) \tag{2.9}$$

Linear Acceleration Method:

$$\dot{u}_{N+1} = \dot{u}_N + \frac{1}{2}\Delta t(\ddot{u}_{N+1} + \ddot{u}_N) \tag{2.10}$$

$$u_{N+1} = u_N + \Delta t\,\dot{u}_N + \Delta t^2(\frac{1}{6}\ddot{u}_{N+1} + \frac{1}{3}\ddot{u}_N) \tag{2.11}$$

The Newmark method generalizes these two solution algorithms by introducing two changeable parameters γ and β. By varying the factors one can adjust numerical stability, accuracy and algorithmic damping.

$$\dot{u}_{N+1} = \dot{u}_N + \Delta t[\gamma \ddot{u}_{N+1} + (1-\gamma)\ddot{u}_N] \tag{2.12}$$

$$u_{N+1} = u_N + \Delta t\, \dot{u}_N + \frac{1}{2}\Delta t^2[2\beta \ddot{u}_{N+1} + (1-2\beta)\ddot{u}_N] \tag{2.13}$$

Unconditional stability, regardless of size of time increment, is achieved if the condition $2\beta \geq \gamma \geq 0.5$ is met (Cook et al., 2002).

2.3 Calculation of dynamic response for cantilever

Ice structure interaction for a line like vertical structure can be modeled as a cantilever beam subjected to a dynamic point load. The equation of motion for a multi degree of freedom system can be described as follows

$$[\mathbf{M}]\{\ddot{\mathbf{u}}\} + [\mathbf{C}]\{\dot{\mathbf{u}}\} + [\mathbf{K}]\{\mathbf{u}\} = \{\mathbf{F}_{ext}\} \tag{2.14}$$

A cantilever is easiest discretized by four degrees of freedom beam elements. Because the loading, generated from the ice, only works on a small area of the structure, it can be applied on one single degree of freedom *i*. The load vector will then consist of zeroes, except from the global ice load F_G in row *i*, as illustrated in Fig. 2.9.

$$\{\mathbf{F}_{ext}\} = \begin{bmatrix} 0 \\ \vdots \\ F_G \\ \vdots \\ 0 \end{bmatrix}$$

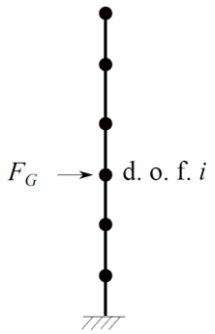

(a) (b)

Figure 2.9 (a) Load vector.(b) Loading in d.o.f. *i.*

The external loading on the cantilever can be calculated as a function of the deformation in the ice. Once the external loading in the given time step is determined, the structural response for each degree of freedom can be solved. An iterative Newmark method routine for calculating the response is presented in Appendix A.

2.4 Rate dependency of ice crushing strength

Ice is known for having varying compressive capacity, depending on the rate of loading. This section presents a brief introduction to the characteristics of ice crushing failure. Expressions for a mathematical description of the behavior are also introduced. Finally, the effect that the rate dependency has on ice induced vibrations is addressed.

2.4.1 Crushing modes

The strain rate dependency of ice crushing strength has been evaluated in several publications e.g. (Peyton, 1968, Michel and Toussaint, 1977, Sodhi, 2001, Sodhi and Haehnel, 2003, Huang and Liu, 2009, Yue et al., 2009, Timco and Weeks, 2009). There exists a general consensus that the failure of ice can be divided into three modes, namely ductile, transition and brittle, as proposed by Michel and Toussaint (1977) . The three domains are illustrated in Fig. 2.10.

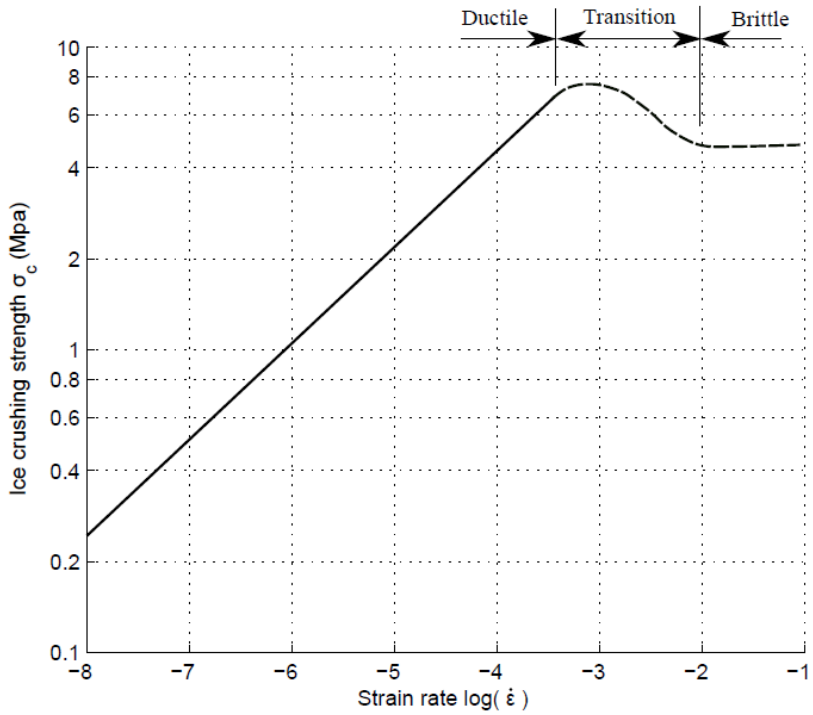

Figure 2.10 Ductile, transitional and brittle failure mode after Michel and Toussaint (1977).

During low strain rates the material conducts ductile failure, meaning that large plastic creep strains and few cracks are observed prior to failure. At high strain rates, several large cracks and hardly any deformation is observed before crushing. The deformation during brittle behavior is primarily elastic as creep strains need more time to develop (Sodhi, 2001). Under medium strain rates the material is in the transition region between ductile and brittle behavior. In this region, small micro cracks propagate in the material. Failure occurs when the cracks connects and the material is saturated (Yue

et al., 2009). The typical time-history force plot during ductile behavior is smooth, whilst it shows abrupt drops during brittle behavior.

2.4.2 Stress rate dependency

The effect of varying crushing capacity at different strain rates can be described by the relation between crushing strength and stress rate. The definition of stress rate has been formulated slightly different by various authors. To define the stress rate in ice when it impinges a cylindrical structure, Blenkarn (1970) used the analogy to an example from contact mechanics presented by Timoshenko and Goodier (1951). Timoshenko and Goodier described the radial stress in a unit thickness plate, loaded on a straight boundary, by the formula given in Eq. (2.15). A sketch of the loading is presented in Fig. 2.11.

$$\sigma = -\frac{2P}{\pi}\frac{\cos\theta}{r} \tag{2.15}$$

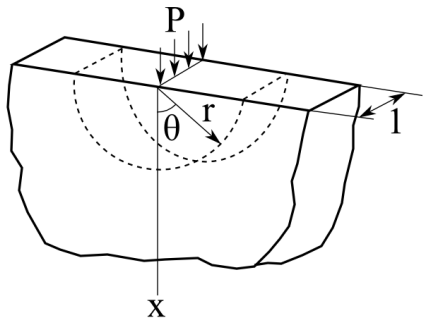

Figure 2.11 Model for calculating radial stress, as described by Timoshenko and Goodier (1951).

It can be shown that there are no shear stresses in the semicircular surface, shown with stapled lines. Blenkarn (1970) therefore suggested that a cylindrical structure could replace a semicircular part of the material. The radial stress in the material at r = structure radius would then represent the contact pressure between ice and structure. Blenkarn modified the equation for radial stress to the following formula

$$\sigma = \frac{4pz}{\pi r}\cos\theta \tag{2.16}$$

The components in eq. 2.16 are illustrated in Fig. 2.12. p equals a loading pressure and z is half the loaded length. Blenkarn's concept of replacing a piece of the material with a cylindrical structure yields that z equals the structure radius and r is the distance from the center of the structure. In the ice structure interface, r equals z.

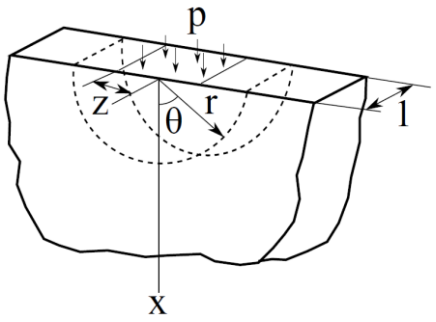

Figure 2.12 Model for calculating radial stress, as described by Blenkarn (1970).

Along the centerline, where θ equals zero, the ice stress rate was then given by

$$\dot{\sigma} = \frac{d\sigma}{dt} = \frac{4pzv_{ice}}{\pi r^2} \tag{2.17}$$

where $v_{ice} = \frac{dr}{dt}$ is the ice velocity.

Määttänen (1998) established a stress rate dependent expression for ice crushing strength, given in Eq. (2.18). The formula employs a polynomial that is approximated to the stress rate dependency measured by Peyton(1968).

$$\sigma_C(\dot{\sigma}) = \begin{cases} (2.00 + 7.80\dot{\sigma} - 18.57\dot{\sigma}^2 + 13.00\dot{\sigma}^3 - 2.91\dot{\sigma}^4)\sqrt{\frac{A_0}{A}}MPa & \text{for } \dot{\sigma} < 1.3\frac{MPa}{s} \\ \sqrt{\frac{A_0}{A}}MPa & \text{for } \dot{\sigma} \geq 1.3\frac{MPa}{s} \end{cases} \tag{2.18}$$

In Eq. (2.18), A is the contact area and A_0 is a reference area. In this way, reduced crushing capacity for wide structures in accordance to area dependence, as defined by Sanderson (1988), is implemented. In Fig. 2.13, the crushing strength by Peyton is illustrated together with the polynomial by Määttänen.

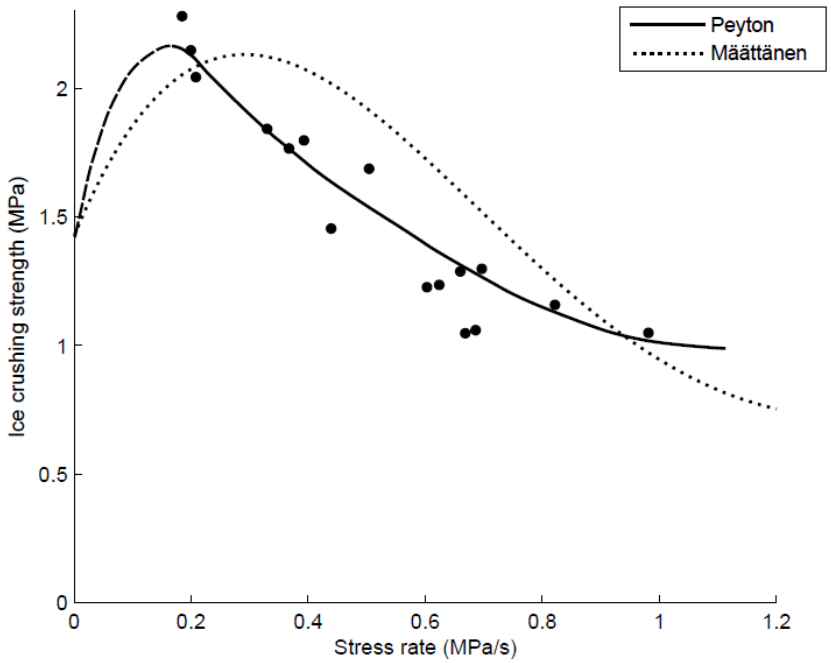

Figure 2.13 Stress rate dependency after Peyton (1968) and Määttänen (1998).

When developing the polynomial, Määttänen used the stress rate definition

$$\dot{\sigma} = (v_{ice} - \dot{u}) \frac{8\sigma_0}{\pi d} \tag{2.19}$$

where v_{ice} is the ice velocity, $\dot{u}$ structure velocity at the interaction point, $A_o = 1m^2$ and $\sigma_0 = 2MPa$. Because the stress rate definition Blenkarn suggested (Eq. (2.17)) is based upon full contact between the ice and the structure, it is best suited for narrow structures where the contact area is similar to the diameter of the structure times the ice thickness. For wider structures, the contact area consists of several scattered contact points at protrusions on the ice edge. Määttänen therefore stated that for wider structures the stress rate could be modified by replacing the contact width *d*, with one to two times the ice thickness. When defining the approximated polynomial he employed *d* = diameter for narrow structures and *d* = 1m for wider structures.

Timoshenko and Goodier (1951) showed that, according to elastic contact theory, the stress varies with the polar angle off the ice drift direction with a cosine distribution . This is illustrated in Fig. 2.14. Due to the variation in stress, the stress rate will also vary over the interaction area. Määttänen (1978) gave the following expression for the stress rate

$$\dot{\sigma} = (v_{ice} - \dot{u}) \cos^2(\theta) \frac{8\sigma_C(\dot{\sigma})}{\pi d} \tag{2.20}$$

Even though it is not stated by Määttänen, the way that Eq. (2.20) is presented, it only gives the stress rate at ice failure, when the stress equals the crushing capacity.

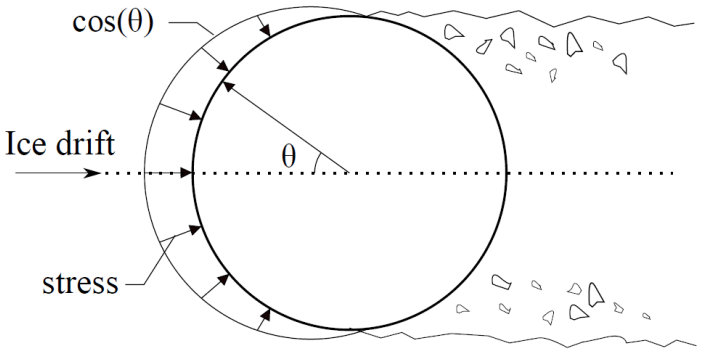

Figure 2.14 Stress distribution over the contact area.

2.4.3 Negative damping

During ice structure interaction, the equation of motion for a single degree of freedom system can be described as

$$M\ddot{u}+C\dot{u}+Ku=F_G(t) \tag{2.21}$$

where *M*,*C* and *K* are mass, damping and stiffness constants, respectively. The global load F_G, is the contact force between the ice and the structure. Because the ice crushing strength is dependent on the loading rate, and the loading rate is dependent on the relative velocity between ice and structure, $F_G=F_G(v_{ice}-\dot{u})$. Assuming small motions, a first order Taylor series expansion of F_G gives

$$F_G(v_{ice}-\dot{u})\approx F_G(v_{ice})+\frac{dF_G}{d\dot{u}}(-\dot{u}) \tag{2.22}$$

Inserting the expression from Eq. (2.22) into the equation of motion gives (Blenkarn, 1970)

$$M\ddot{u}+(C+\frac{dF_G}{d\dot{u}})\dot{u}+Ku=F_G(v_{ice}) \tag{2.23}$$

If the term $\frac{dF_G}{d\dot{r}}$ attains a negative magnitude greater than the damping constant C, negative damping is achieved. Negative damping will lead to dynamic instability of the system, and growing fluctuation amplitudes (Määttänen, 1978).

2.5 Calculation of frequency content

This section introduces methods for establishing the frequency content of a discrete signal, such as force or acceleration measured in full scale.

2.5.1 Fourier Transformation

A continuous signal can be transformed into a sum of harmonic components. This is known as a Fourier transformation. The Fourier transformation takes the signal from the time domain to the frequency domain. The following formulae describe the transformation (Strømmen, 2010);

$$x(t) = \lim_{N\to\infty} \sum_{k=1}^{N} X_k(\omega_k, t) \tag{2.24}$$

$$X_k(\omega_k, t) = c_k \cos(\omega_k t + \phi_k) \tag{2.25}$$

where ω_k is the angular frequency, t is the time, $c_k = \sqrt{a_k^2 + b_k^2}$ and $\phi_k = \arctan\left(\frac{b_k}{a_k}\right)$. The constants a_k and b_k are given by

$$a_k = \frac{2}{T}\int_0^T x(t)\cos(\omega_k t)dt \tag{2.26}$$

$$b_k = \frac{2}{T}\int_0^T x(t)\sin(\omega_k t)dt \tag{2.27}$$

where $\omega_k = k\Delta\omega$, $\Delta\omega = \frac{2\pi}{T}$ and T is the length of the time series.

For a discrete signal, the Fourier transformation can be executed by an algorithm called the Fast Fourier Transform (FFT).

2.5.2 Auto spectral density

The auto spectral density of a signal gives insight into the variance distribution of the signal in the frequency domain. The single sided auto spectrum in a continuous format is given by

$$S_x(\omega) = \lim_{T\to\infty}\lim_{N\to\infty} \frac{E_a\left[X^2(\omega,t)\right]}{\Delta\omega} \tag{2.28}$$

where $X(\omega,t)$ is a Fourier component of the signal $x(t)$. The E_a stands for the average value of the content in the brackets (Strømmen, 2010).

The auto spectral density can be obtained by employing Welch's method. Welch's method removes noise, by reducing the variance in the signal, and produces a smoother spectral density function. The

method implies dividing the signal into several overlapping segments, before performing a Fast Fourier Transform for each segment (Stranneby, 2001).

2.6 Integration of acceleration signal

When integrating a wide banded signal, amplitudes of the parts of the signal with lowest frequencies will increase more than those of higher frequency. If the integration constants are not known, low frequency content will cause drift in the integrated signal. By performing a Fast Fourier Transform (FFT) of an acceleration signal, one can observe the frequency contents. The parts of the signal with frequencies significantly lower than the first natural frequency of the structure can be considered non-relevant when the dynamics of the system is being evaluated. A high pass filter effect can be achieved by removing this unwanted low frequency content and then performing an inverse FFT. A cumulative trapezoidal numerical integration can then be applied to get the velocity $\dot{u}(t)$. The same procedure can be applied before integrating the velocity to find the structural response $u(t)$.

2.7 Estimation of damping

During ice induced vibrations, both structural damping and damping contribution from the ice and water will affect the response of the structure. Due to the strain rate dependency of ice crushing strength, the effect the ice has on damping will depend on the relative velocity between the ice and the structure. This strain rate dependency of the ice crushing strength makes the damping properties of the system constantly change during each fluctuation cycle.

The damping present during FLC is difficult, if not impossible, to quantify in an exact manner. Gravesen et al. (2005) calculated that during oscillations in ice covered waters, the ice contributes to a significantly increased damping. Sodhi (1991) described the energy exchanges between ice and structure during indentation tests. He clearly shows how energy is dissipated from the system when the indentor crushes the ice. Because the ice has an influence on the damping, damping during FLC is different from damping during free vibrations. If a response signal from a structure is available, modal damping can be estimated for vibrations under the governing conditions. This can be done with for instance the *half power method*. The half power method, presented in Eq. (2.29), uses the outline of the frequency response function to estimate the damping ratio ζ_n of a mode *n* (He and Fu, 2001). This is illustrated in Fig. 2.15.

$$\zeta_n = \frac{f_b^2 - f_a^2}{4 f_r^2} \tag{2.29}$$

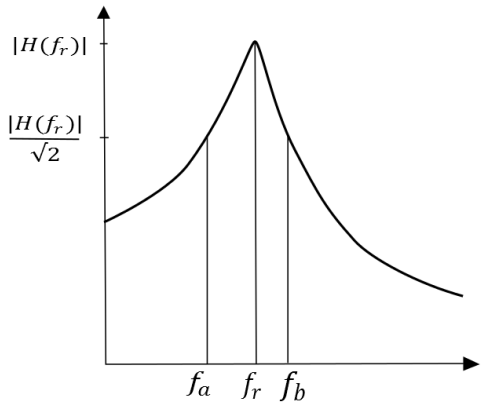

Figure 2.15 Half power method, where $H(f)$ is the frequency response function.

For a real life structure, where the frequency response function is unknown, the spectral density of the acceleration signal can be utilized. The acceleration- and response auto spectrums has the following relation (Strømmen, 2010)

$$S_u(\omega_k) = \frac{S_{\ddot{u}}(\omega_k)}{\omega_k^4} \tag{2.30}$$

By taking the square root of the response auto spectrum, a function that represents the measured response amplitudes in the frequency domain is obtained (Rönnquist, 2005). The half power method can be applied on this function. This is possible because when calculating the modal damping ratio by the half power method, the actual amplitude of the frequency response function is irrelevant, as the damping is obtained as the ratio between values from the same function.

2.7.1 Rayleigh damping

Rayleigh damping can be used to establish a damping matrix. The Rayleigh damping matrix given by the expression

$$[\mathbf{C}] = \alpha_0[\mathbf{M}] + \alpha_1[\mathbf{K}] \tag{2.31}$$

where $[\mathbf{M}]$ is the mass matrix and $[\mathbf{K}]$ is the stiffness matrix. The coefficients α_0 and α_1 can be determined by specifying modal damping ratios ζ_i and ζ_j for two arbitrary natural modes of the structure. Usually, the first damping ratio ζ_i is specified for the fundamental mode and ζ_j for a mode close to the highest mode of significance. The modes in between the selected ones will then be slightly lower damped than ζ_j. Modes higher than the highest mode for which the damping is

specified will get higher damping than ζ_j. Formulas for α_0 and α_1 are given in Eqs. (2.32) and (2.33)(Chopra, 2011).

$$\alpha_0 = 2\omega_i\omega_j \frac{\zeta_i\omega_i - \zeta_j\omega_i}{\omega_j^2 - \omega_i^2} \tag{2.32}$$

$$\alpha_1 = 2\frac{\zeta_j\omega_j - \zeta_i\omega_i}{\omega_j^2 - \omega_i^2} \tag{2.33}$$

A modal analysis must be performed in order to determine ω_i and ω_j, which are the natural frequencies in rad/s, for the selected modes. Estimates to damping ratios for the two selected modes have to be made.

2.8 Description of finite element program

The engineering company REINERTSEN AS has initiated a research program of which results are aimed to contribute during offshore and subsea structural design in ice infested waters. The program is named REice and covers among others, ice crushing loads and ice induced vibrations. As a part of the research program, development of a finite element procedure for calculating structural response during ice induced vibrations has been started. During the work on this thesis, the finite element program has been further developed.

Development of the finite element program has been a significant part of the thesis process. The program is written in the programming language Python. Structural properties are discretized by the means of quite simple beam elements, while the complexity in the program lies in establishing a load implementation that recreates the behavior of true ice. An iterative Newmark method procedure is employed for solving the dynamic equilibrium equations.

2.8.1 Program structure

The program consists of an input file in text format (.txt) and three python scripts (.py). A flowchart illustrating the solving process is shown in Fig. 2.16. It should be mentioned that the program is not developed for general structures. The current version is specifically made for cantilever like structures in a 2D format.

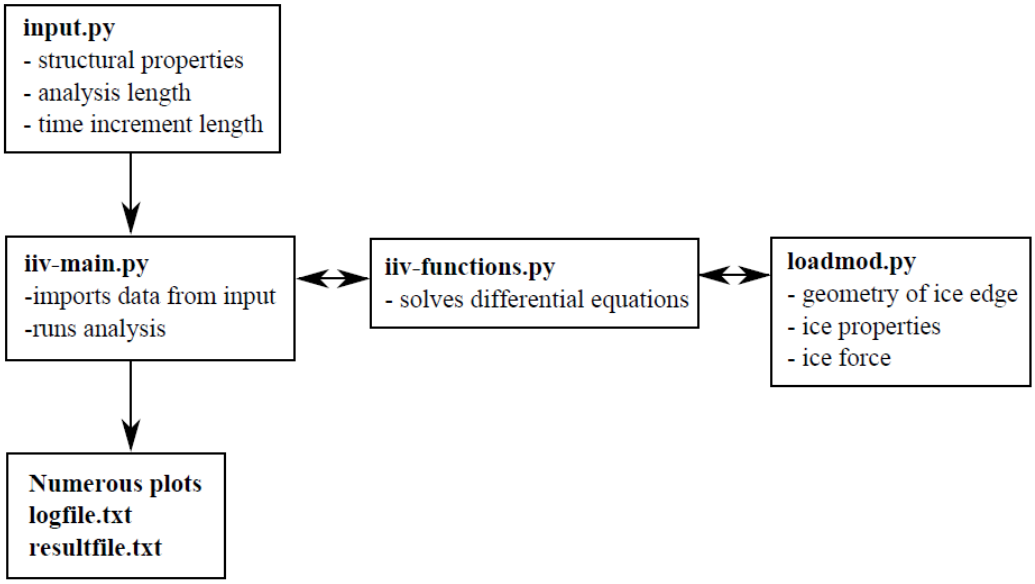

Figure 2.16 Structure of finite element program.

In the input file, the structural properties such as mass, stiffness and damping are given. In addition, the duration of the simulation time and the length of the time increments are defined here.

IIV-main.py loads relevant data from the input file. This script is the hub for the analysis, and runs the functions described in other modules.

In *IIV-functions.py* the differential equations of motion for the structure are solved for each time step. Because the ice force loading is highly non-linear and also dependent of the structural response, an iterative Newmark method scheme is employed.

The contact force over the ice structure interaction area is calculated in *loadmod.py*. Structure geometry and the mechanical properties of ice are included to give the most accurate description possible.

2.8.2 Structural discretization

The tower like lighthouse has axisymmetric properties and is therefore simplified by a 2D representation. Due to varying mass- and stiffness properties over the height, the structure is divided into twenty sections. Each section is implemented by one or more four degrees of freedom Timoshenko beam elements. In total the structure is divided into 99 elements and consists of 200 degrees of freedom, but the mesh density can easily be adjusted. The element distribution is presented in Table 2.2. The mass density of some of the sections is adjusted to compensate for ballast, bulkheads and interior. Calculation of compensating densities is presented in Appendix D. Hydrodynamic added mass and aerodynamic added mass are neglected.

Section	Length (m)	Elements	Outer diam. (m)	Wall thickn. (m)	E (N/mm²)	ρ (kg/m³)
1	7.45	10	23.0	0.52	24000	24935
2	9.05	10	7.2	0.5	24000	8520
3	2.90	10	5.3	0.55	24000	2650
4	0.20	1	4.2	2.1	24000	2500
5	2.90	10	5.0	0.55	24000	2650
6	0.20	1	4.2	2.1	24000	2500
7	2.90	10	5.0	0.55	24000	2650
8	0.20	1	7.7	3.85	24000	2500
9	2.25	10	4.8	0.3	24000	2650
10	0.20	1	4.2	2.1	24000	2500
11	2.25	10	4.8	0.3	24000	2650
12	0.20	1	4.8	2.4	24000	2500
13	2.70	5	4.6	0.25	24000	2650
14	0.20	1	4.2	2.1	24000	2500
15	2.70	5	4.6	0.25	24000	2650
16	0.20	1	4.2	2.1	24000	2500
17	2.70	5	4.6	0.25	24000	2650
18	0.20	1	6.8	3.4	24000	2500
19	2.75	5	4.6	0.25	24000	2650
20	0.20	1	8.5	4.25	24000	2500
Sum	42.35	99				

Table 2.2 Element distribution and details.

Timoshenko beam element differs from the more traditional Euler-Bernoulli element by including shear deformations (Cook et al., 2002). Shear deformations have a greater influence the larger the length to height ratio of the structure. For structures with ratio less than 5, shear deformations will have a significant influence, so for a partially wide structure like Norströmsgrund, shear deformations should be included. The element stiffness matrix is taken from Gavin (2014);

$$[\mathbf{k}] = EI \begin{bmatrix} \frac{12}{l^3(1+\Phi)} & \frac{-6}{l^2(1+\Phi)} & \frac{-12}{l^3(1+\Phi)} & \frac{-6}{l^2(1+\Phi)} \\ \frac{-6}{l^2(1+\Phi)} & \frac{4+\Phi}{l(1+\Phi)} & \frac{6}{l^2(1+\Phi)} & \frac{2-\Phi}{l(1+\Phi)} \\ \frac{-12}{l^3(1+\Phi)} & \frac{6}{l^2(1+\Phi)} & \frac{12}{l^3(1+\Phi)} & \frac{6}{l^2(1+\Phi)} \\ \frac{-6}{l^2(1+\Phi)} & \frac{2-\Phi}{l(1+\Phi)} & \frac{6}{l^2(1+\Phi)} & \frac{4+\Phi}{l(1+\Phi)} \end{bmatrix} \tag{2.34}$$

where E is Young's modulus, I is the second moment of area, l is the element length, $\Phi = \frac{24}{\kappa}(1+\nu)\left(\frac{q}{l}\right)^2$, ν = Poisson's ratio and $q = \sqrt{\frac{I}{A}}$. For Hollow circular cross sections the shear coefficient κ can be calculated by Eq. (2.35) (Cowper, 1966).

$$\kappa = \frac{6(1+\nu)(1+n^2)^2}{(7+6\nu)(1+n^2)^2 + (20+12\nu)\mathrm{n}^2} \tag{2.35}$$

where $n = \frac{b}{a}$ gives the relation between inner and outer radius, as shown in Fig. 2.17.

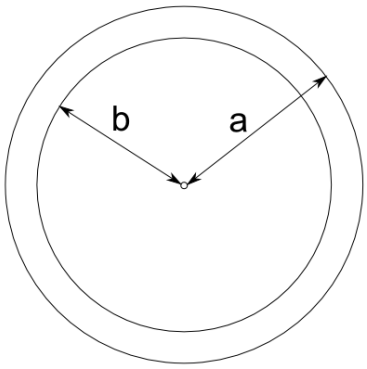

Figure 2.17 Inner and outer radius.

A consistent mass matrix is applied in the discretization. Consistent mass matrices over-estimate the natural frequencies. This partially compensates for the algorithmic error of period elongation that explicit direct integration cause (Cook et al., 2002).The shape functions used to calculate the element mass matrix includes the shear deformations. Eq. (2.36) gives the element mass matrix (Gavin, 2014).

$$[\mathbf{m}] = m\begin{bmatrix} \frac{156}{420}+\frac{7}{10}\Phi+\frac{1}{3}\Phi^2 & -l\left(\frac{22}{420}+\frac{11}{120}\Phi+\frac{1}{24}\Phi^2\right) & \frac{54}{420}+\frac{3}{10}\Phi+\frac{1}{6}\Phi^2 & l\left(\frac{13}{420}+\frac{3}{40}\Phi+\frac{1}{24}\Phi^2\right) \\ -l\left(\frac{22}{420}+\frac{11}{120}\Phi+\frac{1}{24}\Phi^2\right) & l^2\left(\frac{4}{420}+\frac{1}{60}\Phi+\frac{1}{120}\Phi^2\right) & -l\left(\frac{13}{420}+\frac{3}{40}\Phi+\frac{1}{24}\Phi^2\right) & -l^2\left(\frac{3}{420}+\frac{1}{60}\Phi+\frac{1}{120}\Phi^2\right) \\ \frac{54}{420}+\frac{3}{10}\Phi+\frac{1}{6}\Phi^2 & -l\left(\frac{13}{420}+\frac{3}{40}\Phi+\frac{1}{24}\Phi^2\right) & \frac{156}{420}+\frac{7}{10}\Phi+\frac{1}{3}\Phi^2 & l\left(\frac{22}{420}+\frac{11}{120}\Phi+\frac{1}{24}\Phi^2\right) \\ l\left(\frac{13}{420}+\frac{3}{40}\Phi+\frac{1}{24}\Phi^2\right) & -l^2\left(\frac{3}{420}+\frac{1}{60}\Phi+\frac{1}{120}\Phi^2\right) & l\left(\frac{22}{420}+\frac{11}{120}\Phi+\frac{1}{24}\Phi^2\right) & l^2\left(\frac{4}{420}+\frac{1}{60}\Phi+\frac{1}{120}\Phi^2\right) \end{bmatrix} \tag{2.36}$$

where m is mass per length unit and l is the element length.

Soil structure interaction is implemented by one rotational and one translational spring. Due to lacking data on soil characteristics from Norströmsgrund, the stiffness of the two springs must be considered approximate. Values are taken from a numerical study by Popko (2014).

$$K_{lat} = 6.0 \cdot 10^{9}\ \text{N/m}$$

$$K_{rot} = 8.0 \cdot 10^{11}\ \text{Nm/rad}$$

2.8.3 Load Module

Response dependent loading on the structure is what separates the program from being an ordinary calculation of forced vibrations. The loading is response dependent because the contact force depends on the displacement in the ice and because the ice capacity is dependent on the relative velocity between ice and structure.

The axisymmetric structure is utilized, as only one half of the interaction area is modelled. One half of the interaction area gives a sector of 90˚ or π/2 rad. This sector is divided into segments of 0.01rad. Each of these segments is discretized to a contact node. In total, the ice structure interaction consists of 158 discrete contact points. A principle sketch of the discretization is shown in Fig. 2.18. Ice stress and deformation is calculated separately for each point, in which the ice is represented by an elastic spring. This means that the model employs 158 separate elastic elements like the one used in the Matlock model (Matlock et al., 1969). The Matlock model is illustrated in Fig. 2.19. One of the strengths of this representation compared to many other ice structure interaction models is that it maintains kinematic compatibility and equilibrium between the ice and the structure (Sodhi, 1988).

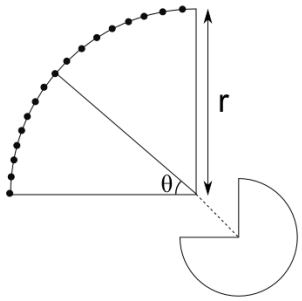

Figure 2.18 Modeled contact points.

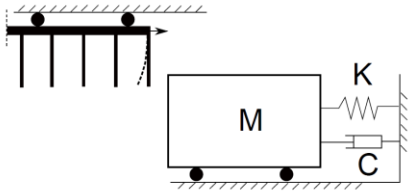

Figure 2.19 The Matlock model on a SDOF system.

By applying Eq. (2.37), the force acting on the structure is calculated for each time step N, by integrating the stress over the polar angle and multiplied by two, accounting for the symmetry utilization. The harmonic terms account for only including the component of the radial normal stress and the tangential shear stress that is working in the ice drift direction.

$$F_G^N = 2hr\int_0^{\frac{\pi}{2}} \sigma^N(\theta)\cos(\theta) + \mu\sigma^N(\theta)\sin(\theta)d\theta \tag{2.37}$$

The Matlock model has proven able to produce structural response similar to what is measured in full-scale. However it does not include any parameters describing the ice properties. In the finite

element model, the ice crushing capacity is calculated as a function of stress rate, by utilizing the description proposed by Määttänen (1998, 1978). A tuning factor φ, is used to control the level of the global load, instead of the scaling term $\sqrt{A_0 / A}$ used in Eq. (2.18). Note that the value *d*, which was used in Eqs. (2.19) and (2.20), is in Eq. (2.39) replaced with 1m, like Määttänen (1998) suggested for wide structures.

$$\sigma_C(\dot{\sigma},\theta) = \sigma_C(\dot{\sigma})\cos(\theta) \tag{2.38}$$

$$\dot{\sigma} = \frac{1}{\varphi}(v_{ice} - \dot{u})\cos^2(\theta)\frac{8\sigma_C(\dot{\sigma})}{\pi 1m} \tag{2.39}$$

$$\sigma_C(\dot{\sigma}) = \begin{cases} \varphi(2.00 + 7.80\dot{\sigma} - 18.57\dot{\sigma}^2 + 13.00\dot{\sigma}^3 - 2.91\dot{\sigma}^4)MPa & \text{for } \dot{\sigma} < 1.3\dfrac{MPa}{s} \\ \varphi MPa & \text{for } \dot{\sigma} \geq 1.3\dfrac{MPa}{s} \end{cases} \tag{2.40}$$

The crushing strength depends on the stress rate, and the stress rate depends on the acting stress. At failure, the stress is equal to the crushing strength as stated in Eq. (2.39). To decide whether the ice fails or not in the current time step N, a predictor-corrector procedure is employed. The stress rate in step N is calculated based on the known stress in step $N-1$. Crushing strength in step N is then calculated from stress rate in step N.

$$\sigma_C^N(\dot{\sigma},\theta) = \sigma_C^N(\dot{\sigma}^N)\cos(\theta) \tag{2.41}$$

$$\dot{\sigma}^N = \frac{1}{\varphi}(v_{ice} - \dot{u}^N)\cos^2(\theta)\frac{8\sigma^{N-1}(\dot{\sigma}^{N-1})}{\pi 1m} \tag{2.42}$$

$$\sigma_C^N(\dot{\sigma}^N) = \begin{cases} \varphi(2.00 + 7.80\dot{\sigma}^N - 18.57(\dot{\sigma}^N)^2 + 13.00(\dot{\sigma}^N)^3 - 2.91(\dot{\sigma}^N)^4)MPa & \text{for } \dot{\sigma} < 1.3\dfrac{MPa}{s} \\ \varphi MPa & \text{for } \dot{\sigma} \geq 1.3\dfrac{MPa}{s} \end{cases} \tag{2.43}$$

In the predictor step, the stress in the ice is calculated based on the current ice displacement δ^N, by applying Eq. (2.44).

$$\sigma^N(\theta) = \frac{K_{eff}\delta^N\cos(\theta)}{2rh\int_0^{\frac{\pi}{2}}\cos^2(\theta) + \mu\cos(\theta)\sin(\theta)\,\mathrm{d}\theta} \tag{2.44}$$

Eq. (2.44) is deducted in Appendix B. K_{eff} is the effective stiffness of the ice giving the relation $F_G = K_{eff}\delta$.

If $\sigma^N > \sigma_C^N$ the ice will fail and the displacement in the ice δ, is reduced, such that $\delta^N = \delta^N - c$, where *c* is a predefined crushing length. In the corrector step, an updated stress then has to be calculated based on the new displacement in the ice. The crushing length will influence the crushing frequency, because it affects how long time it will take before the stress reaches the crushing capacity again. A thorough description of the calculations in the load module is given in Appendix C.

3 Results

In this chapter, features describing the characteristics of the dynamic response of Norströmsgrund lighthouse during the 30031225 FLC-event are presented. Results from two numerical simulations of the event are also given. In the first numerical simulation, the 30031225 FLC-event is recreated by performing a finite element analysis where the loading is tuned to be similar to the loading measured in full-scale. In the second numerical simulation, it is attempted to achieve dynamic response as a result of negative damping effects. Both analyses are performed with the same finite element program, but the equations describing ice properties are slightly different in the two analyses.

3.1 Documentation of lock-in characteristics

It should be verified that the event we are assessing is indeed a true frequency lock-in event. For a period of about 80 seconds the global load, presented in Fig. 3.1(a), reaches exceptionally high values. The structural acceleration, shown in Fig. 3.1(b), is significant during the same interval. This interval is what has been named *FLC event.* An interval prior to lock-in is denoted *Pre event.*

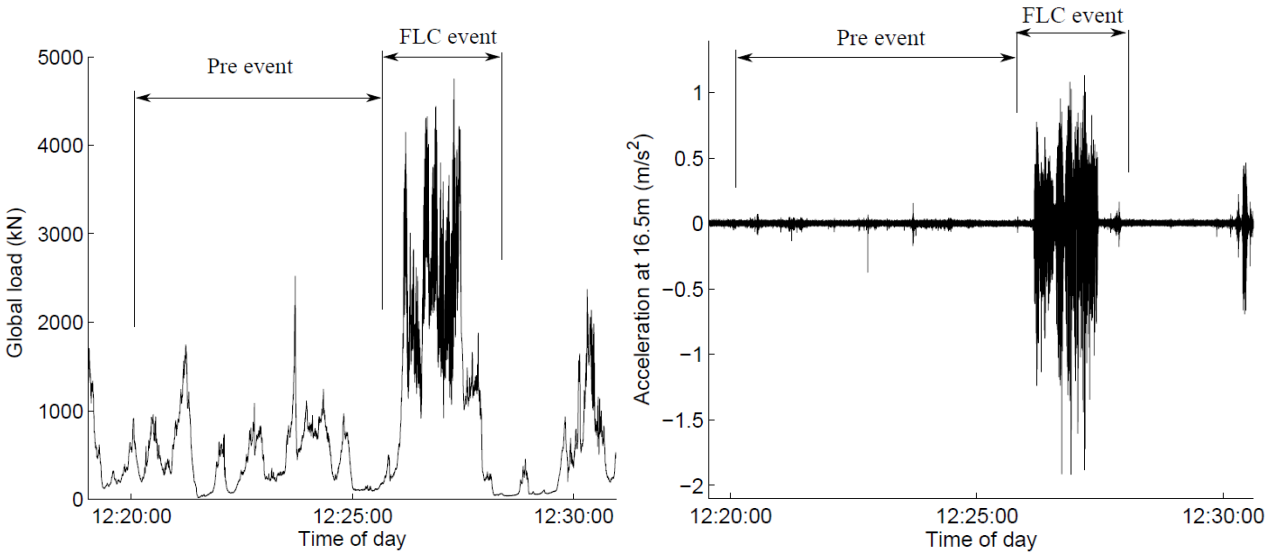

(a) (b)

Figure 3.1 (a) Global load before and during FLC event. (b) Acceleration before and during FLC event.

An assessment of the frequency content of the acceleration signal during the FLC event, given in Fig. 3.2(a), shows that the vibrations are dominated by the first eigenmode of the structure, at about 2.2Hz. For comparison, the time period prior to the lock-in event is assessed in Fig. 3.2(b). During this period, named Pre event, the frequency content is more wide-banded than during the FLC event. In the pre event there is a dominating frequency at about 37Hz, which is just below the Nyquist frequency of 42Hz. It has not been succeeded to determine if the energy at 37Hz is due to noise or a

physical process. Because there is no energy at 37Hz during the FLC event, it is not regarded significant for this work to investigate this energy further. It should, however, be looked into what the energy at this frequency stems from.

The loading during the Pre event can be characterized as intermittent crushing, due to the gradual load increases followed by sudden decreases to a load level that remains low for some time. The frequency of the first natural mode is at 2.7Hz in the Pre event and 2.2Hz during the FLC event. This indicates that the frequency during FLC is not equal to the natural frequency during free vibrations.

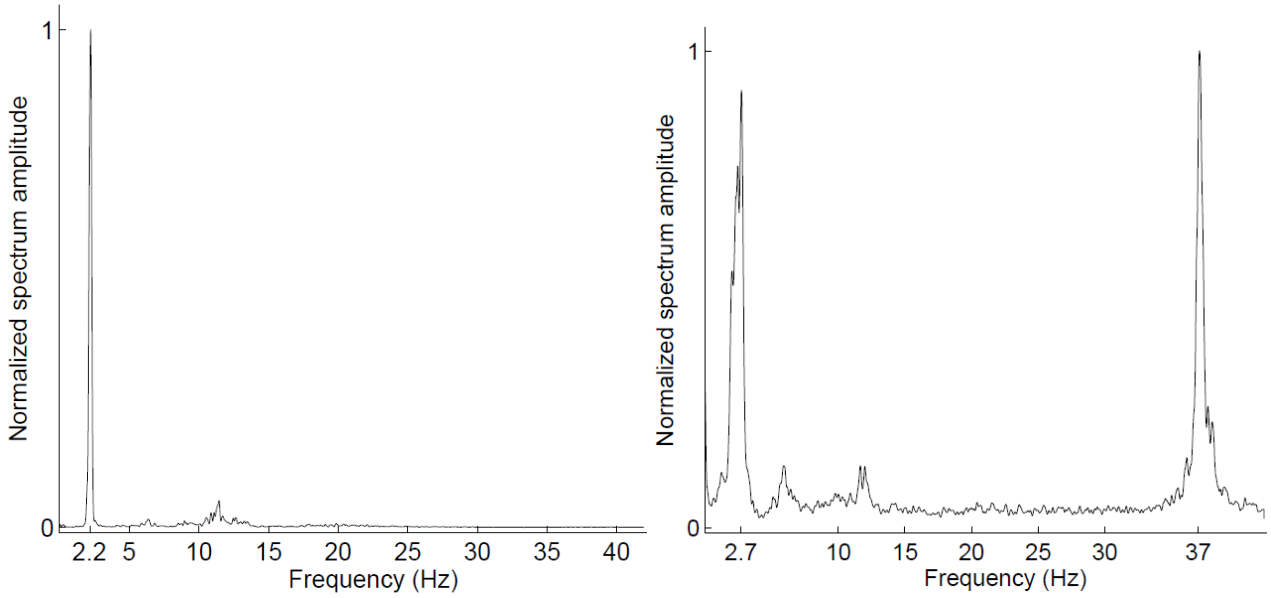

(a) (b)

Figure 3.2 (a) Acceleration auto spectrum of FLC event. (b) Acceleration auto spectrum of Pre event.

Fig. 3.3 shows the auto spectrum of the global load during the FLC event. The dominating frequency is at about 2.2Hz. There is also some energy at 4.4Hz and 6.6Hz. The energy at 2.2Hz is deemed to come from the first vibration mode, while the energy at 4.4Hz and 6.6Hz possibly comes from higher order modes or from a superharmonic oscillation of the first mode. Local effects due to vibrations in the load panel itself can be another explanation to the energy at higher frequencies.

The displacement signal in Fig 3.4 shows how the oscillations are very harmonic, and mainly consists of a single frequency. Steady-state response is an indicator of frequency lock-in and the relatively stable amplitudes of the displacements are in line with this.

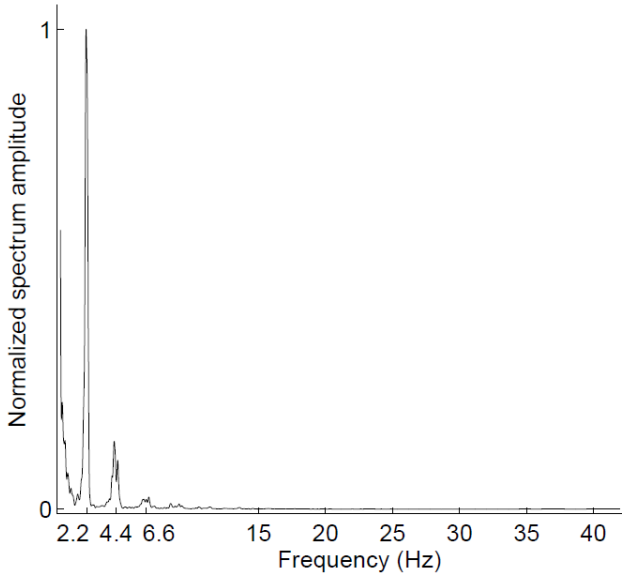

Figure 3.3 Auto spectrum of global load signal

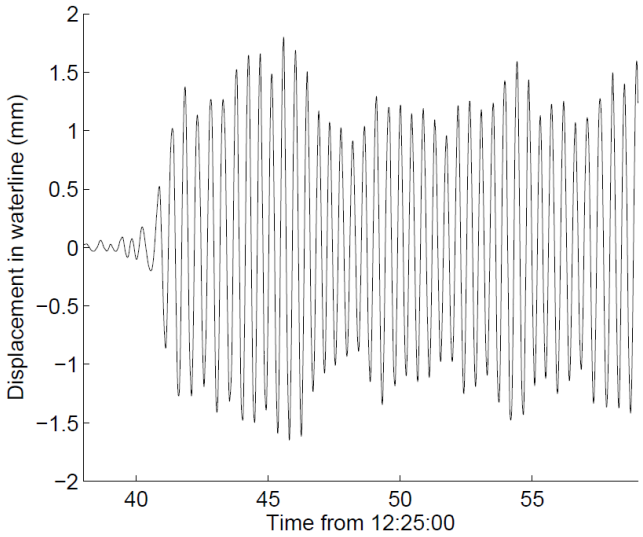

Figure 3.4 Steady state structural response.

It should be mentioned that the frequency of the measured structural response varies over the event. During the first seconds of lock-in, the dominating frequency is about 2.17Hz, while when evaluating the entire event, a frequency of 2.23Hz is most dominant. Some deviating values will therefore appear in the report.

By visually examining the force panel measurements it becomes clear that crushing is synchronized over the interaction area. This can be examined in Fig. 3.5.

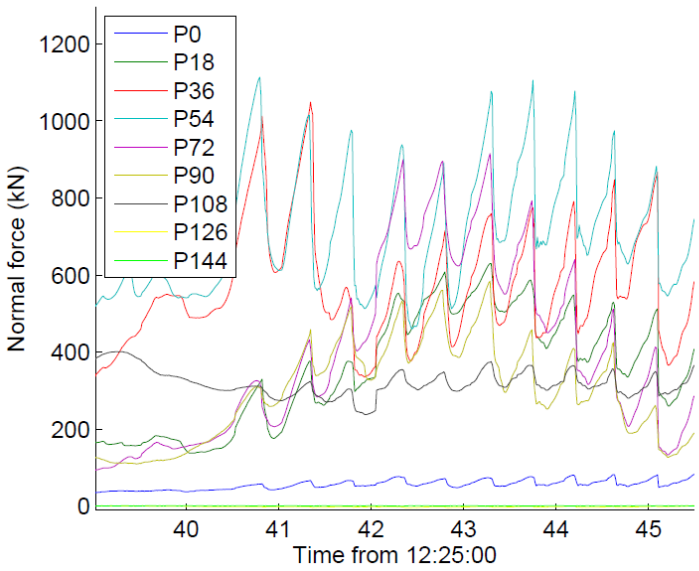

Figure 3.5 Synchronized panel forces.

It has been showed that the interval of vibrations, denoted as the 30031225 FLC-event, consisted of steady-state harmonic oscillations at a frequency of 2.2Hz. The ice failure was synchronized over the interaction area during the interval.

3.2 Study of initiation of forces during the 30031225 FLC-event

Recordings from the 30031225 FLC-event have been evaluated in order to assess how the shape and movement of the ice sheet influence the loading on the structure. Camera recordings reveal how a semicircular crack in the ice sheet was approaching the structure prior to the initiation of vibrations. The shape and movement of the crack is depicted on snapshots from the video recordings in Fig. 3.6. Each black line illustrates the shape and position of the crack for each point of time. Governing minute and second for each line is included in the figure. On figure 3.6(b) a secondary crack can be seen. It has not been discovered how this crack affects forces on the structure.

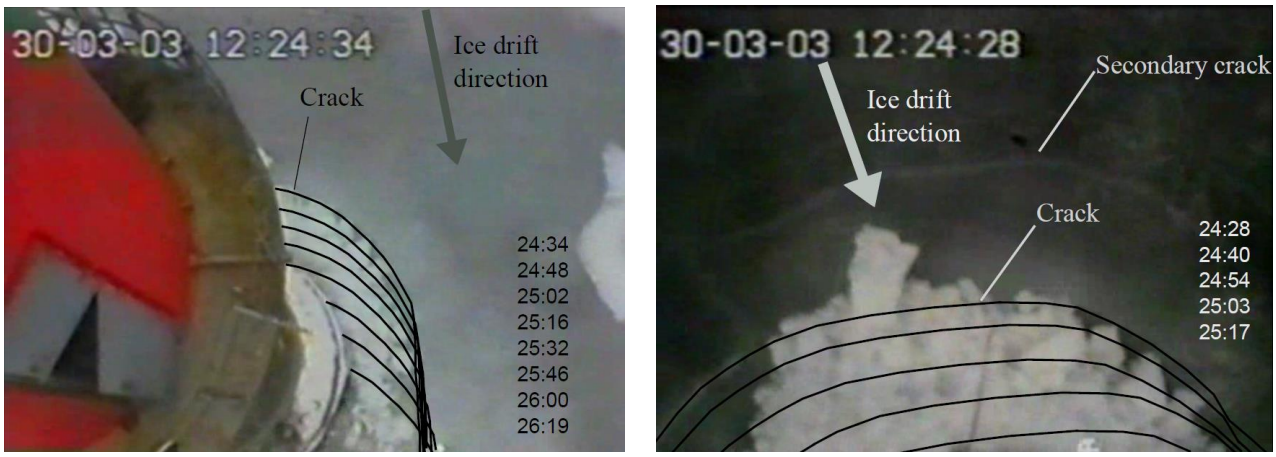

(a) (b)

Figure 3.6 Ice edge time history

From the video recordings one can make at least two relevant observations. 1) The radius of the crack is larger than the radius of the lighthouse. This indicates that the force build up most possibly should begin in the mid force panels before gradually spreading out along the perimeter. 2) The edge of intact ice gains contact with the lighthouse at about 12:25:32. Both of these observations are in accordance with what the force panel measurements show.

A possible sequence of events has been established to recreate the load measurements. This is a potential shape of the ice edge, tuned to give a time history that corresponds to the force panel readings. In Fig. 3.7 the outline of the ice front has been sketched.

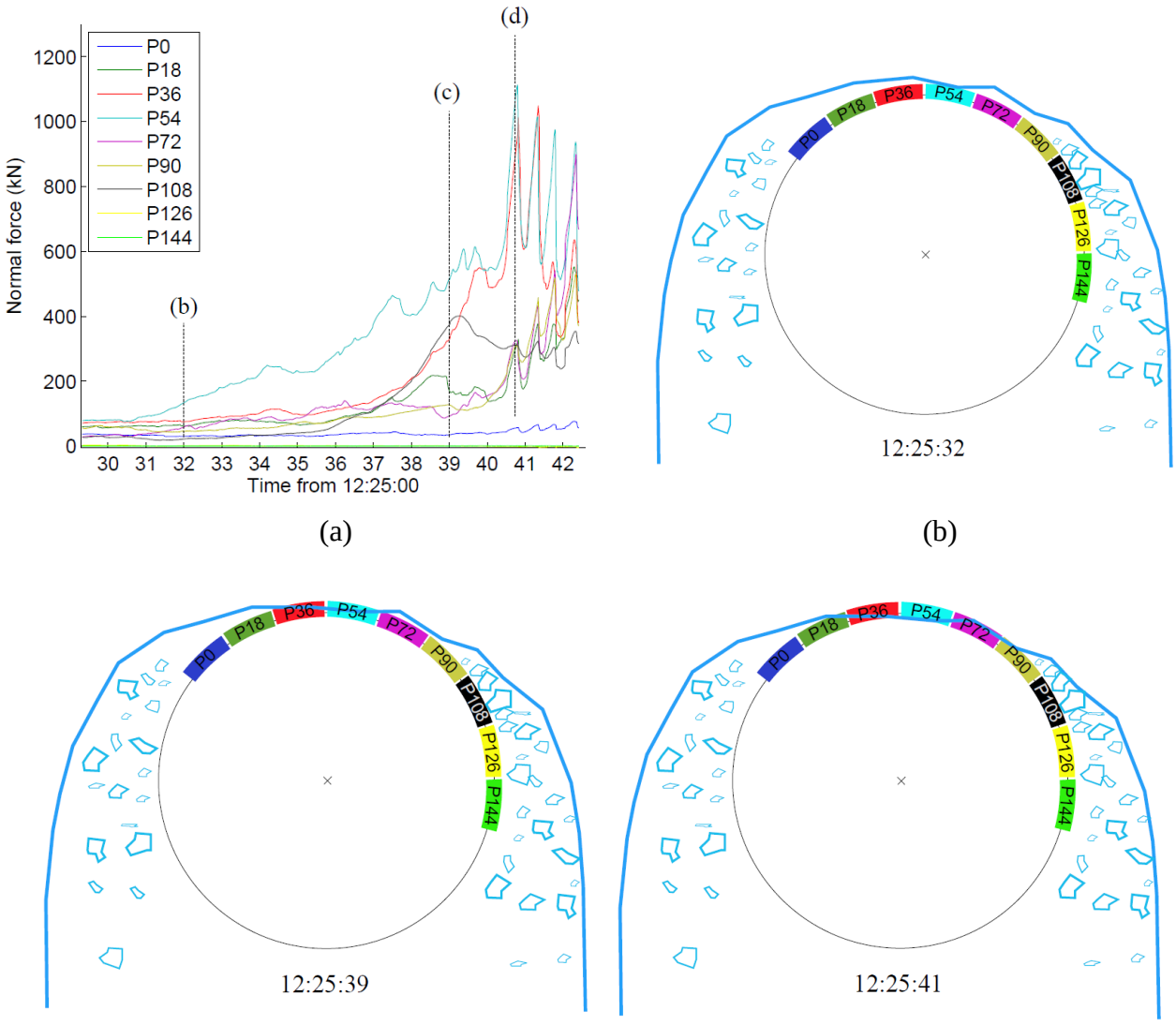

Figure 3.7 (a) Force panel time history. (b) Initial contact is made. (c) Contact is gained for panel P36 and rubble causes forces on P108. (d) Contact at a substantial part of the perimeter.

It has been created an image of how the ice impingement of the structure led to development of contact forces. A course of events where contact between structure and ice, to begin with, is gained in front of the structure, before gradually spreading out to the sides, can explain the force measurements.

3.3 Correlation between load and response

In this section the correlation between loading and structural response is assessed.

In Figs. 3.8 and 3.9, global ice loads are plotted together with displacements and relative velocity, respectively. The amplitudes are scaled to give a perspective that enables comparison. The displacement and velocity are obtained by integrating the acceleration measurements. Low frequency

content is lost during the integration, so the plots will only show the dynamic response. Hence, quasi static response due to increasing load is not captured in the displacement signal.

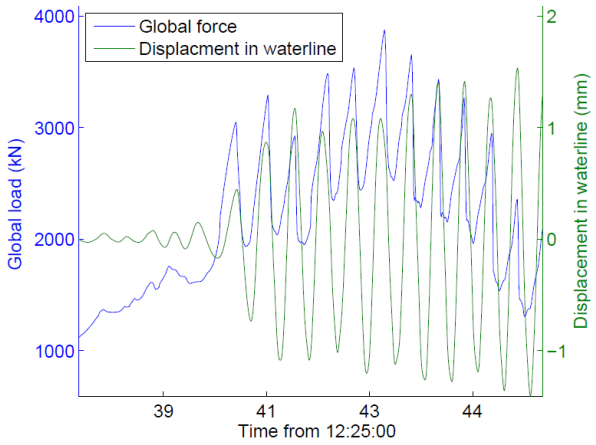

Figure 3.8 Global load and displacement.

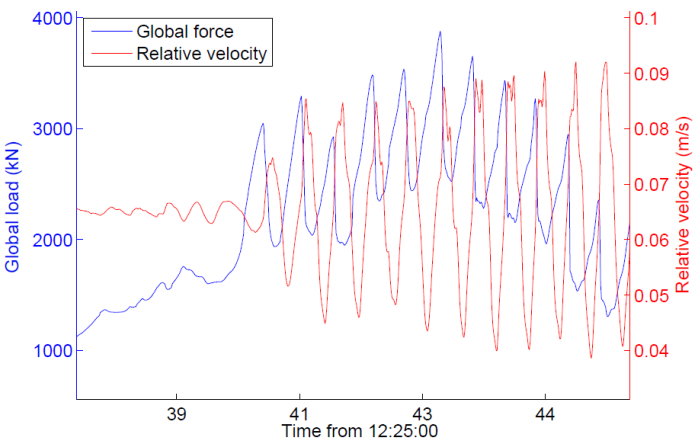

Figure 3.9 Global load and relative velocity.

The force and displacement are in phase during the vibrations. The relative velocity, being the difference between ice velocity and structure velocity, behaves like the negative derivative of the displacement. Note that the relative velocity is fluctuating about a mean equal to the ice velocity at 0.065m/s. For each cycle one can observe that while the force and displacement is increasing, the relative velocity is low. This is reasonable, because when the structure deforms, it moves together with the ice edge, reducing relative velocity. When the force reaches its maximum value, the displacement also tends to have reached its climax. At this point the derivative of the displacement is zero. The relative velocity therefore has a value about equal to the ice velocity, at ice failure. When the ice fails, the structure penetrates the ice sheet, and the relative velocity increases.

The relationship between translation of the ice sheet, contact force and displacement of the structure has been investigated closer. Fig. 3.10 shows four specific points on the displacement signal, indicating zero, minimum and maximum displacement during one fluctuation cycle.

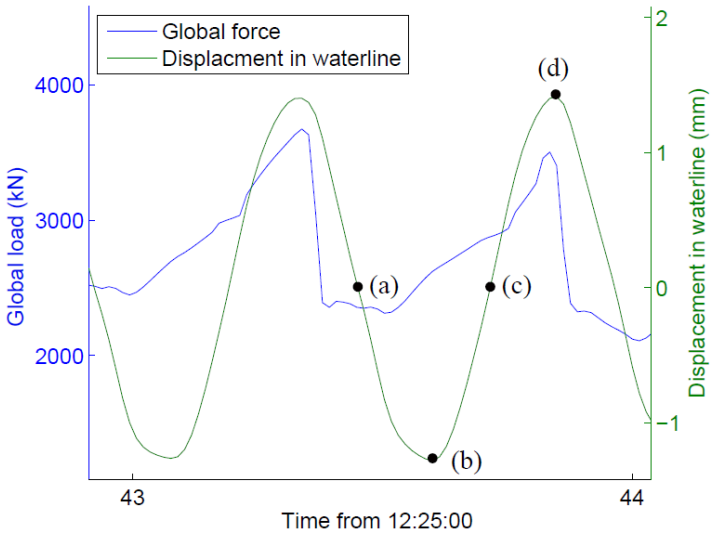

Figure 3.10 Specific points in displacement signal.

For each of the four points, the movement of the ice sheet is, in Fig. 3.11, illustrated together with the displacement of the lighthouse. The movement of the ice sheet is calculated by multiplying the ice velocity with the elapsed time. For the purpose of illustrating the movement of the ice sheet, it has in the figure been divided into a rigid and a deformable part.

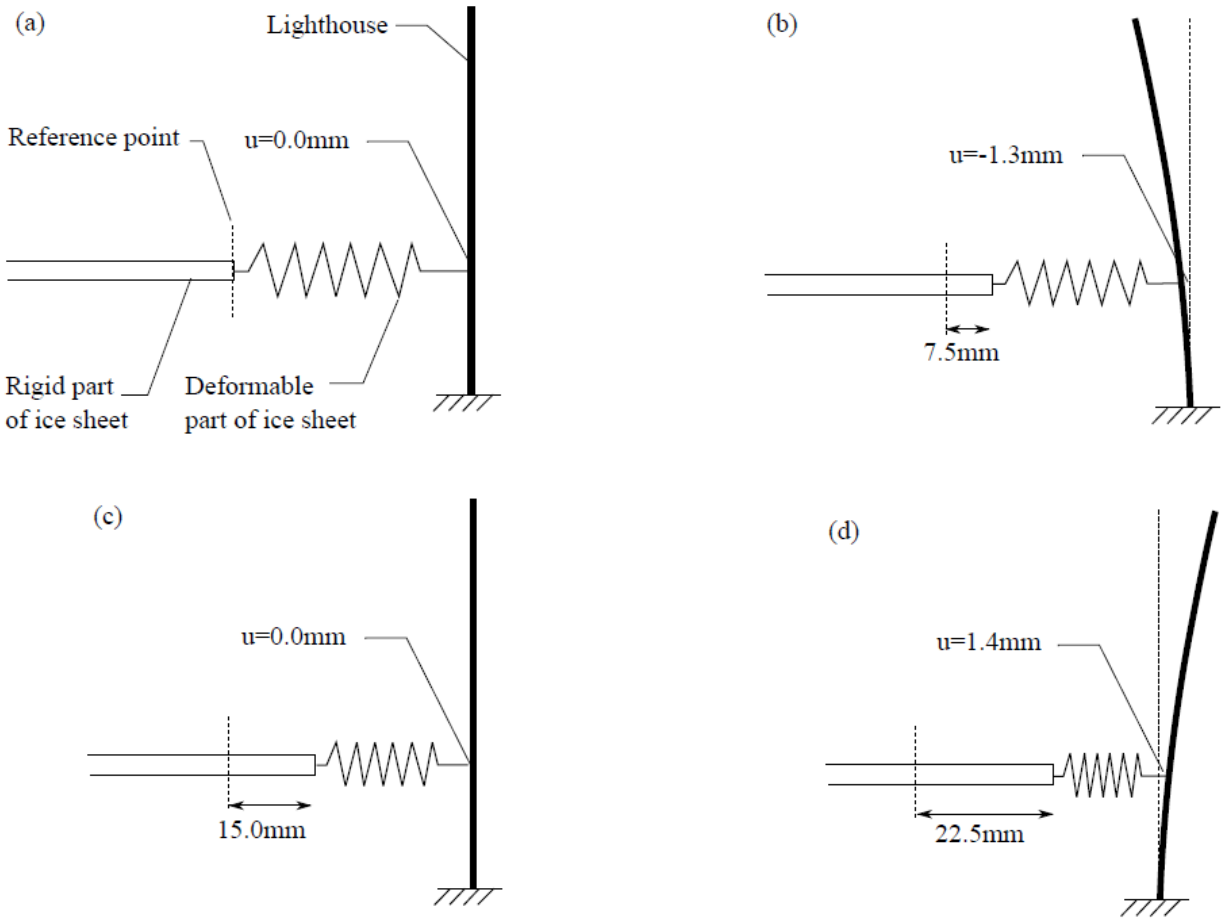

Figure 3.11 Relation between movement of ice sheet and deformation of the lighthouse.

In point (a) the deformation in the structure is zero and the force is in the beginning of a load build up. From point (a) to (b), the ice moves 7.5mm and the structure moves 1.3mm against the direction of the ice. In point (c) the structure has moved back to its neutral position, and in point (d) the structure has reached its maximum displacement of 1.4mm in the direction of the ice. Point (d) also marks the end of the force build up. During the load build up, the relative movement between ice sheet and structure is approximately 22.5mm-1.4mm=21.1mm. Assuming entirely elastic behavior, this means that the ice undergoes a deformation of 21.1mm during this cycle. For the load to reduce to the level it had prior to the load build up, the crushing length of the ice has to be approximately equal to the deformation of 21.1mm.

3.4 Development of force distribution during initiation

It is of interest to assess how the force distribution in the ice structure interaction is developing, as the vibrations evolve. Therefore, eleven readings in the force panel measurements have been made at specific points of time. The horizontal force distribution at each force reading has then been plotted and compared with each other. Fig. 3.12(a) shows when the eleven force readings were made. Force distributions are presented in Figs. 3.12(b) to 3.12(d).

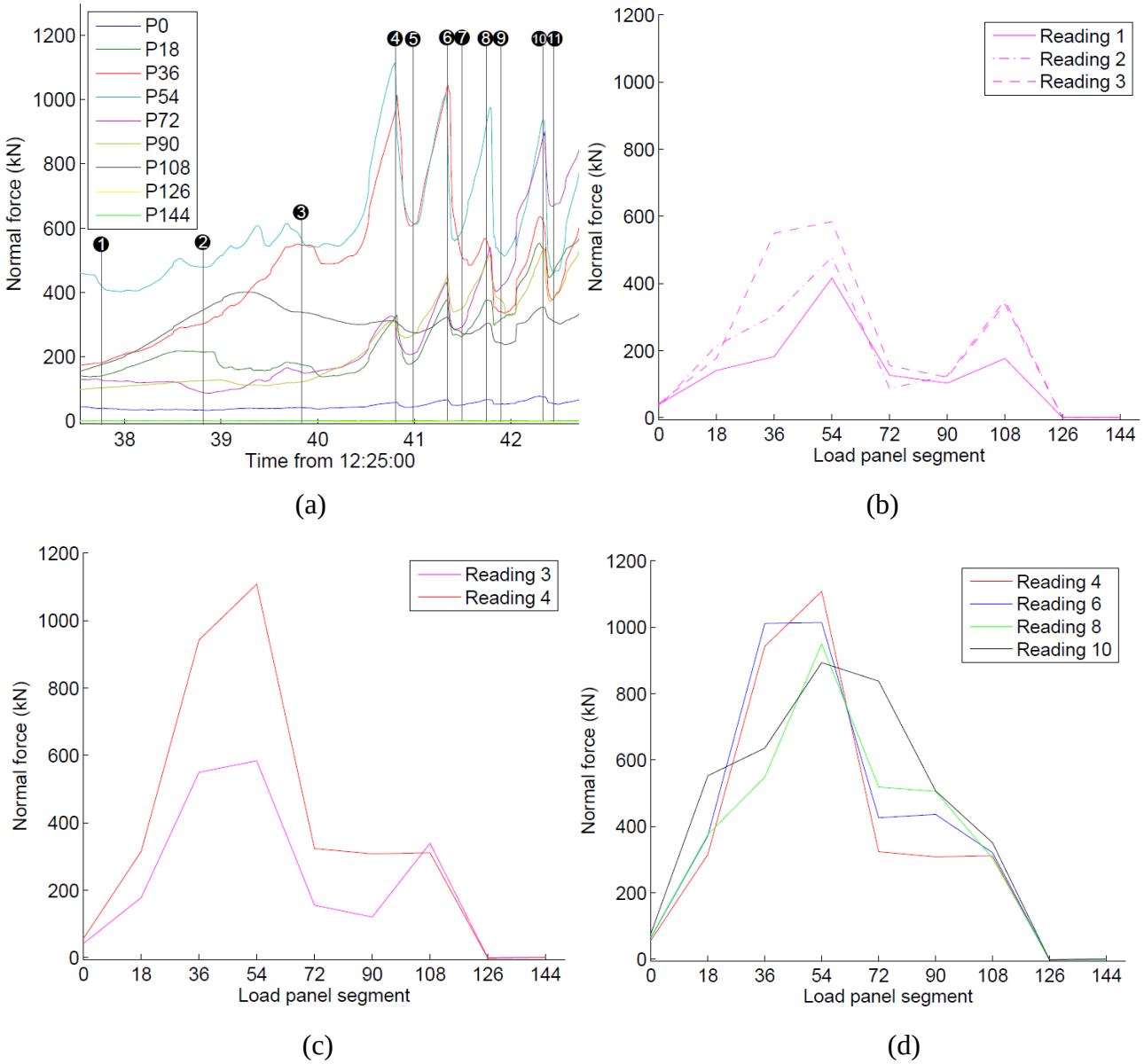

Figure 3.12 (a) Time of force readings. (b) Distributions during quasi-static load increase. (c) Distributions before and after global load increase. (d) Distributions at force maxima.

From readings 1, 2 and 3 one can see the force development prior to the start of the vibrations. The average rate of load increase is low in this period. Between reading 1 and 3 the loading rate is about 80kN/s for panel P54 and about 120kN/s for P36. The load is concentrated around the center of the structure, in addition to a smaller force on panel P108.

Between reading 3 and 4, there is a significant increase in the global load. Fig. 3.12(c) shows how the main increase in load primarily occurs in the two mid panels.

In Fig. 3.12(d) the distribution at the different force maxima during the first cycles of the vibrations are compared. The trend is that the distribution develops from being concentrated at the mid panels

to at more cosine like distribution. From reading 4 to reading 10, the force decreases in the mid panels P36 and P54, while it increases in panel P18, P72 and P90.

Finally the development between force maxima and minima are assessed. In Figs. 3.13(a) and (b) it can be observed that the fluctuations in force are most prominent in the two mid panels P36, P54. The relative difference between maximum and minimum values is significant in these panels. In the panels P18 and P72 the fluctuations are smaller, while the fluctuations of the force in panels P0 and P18 are almost absent.

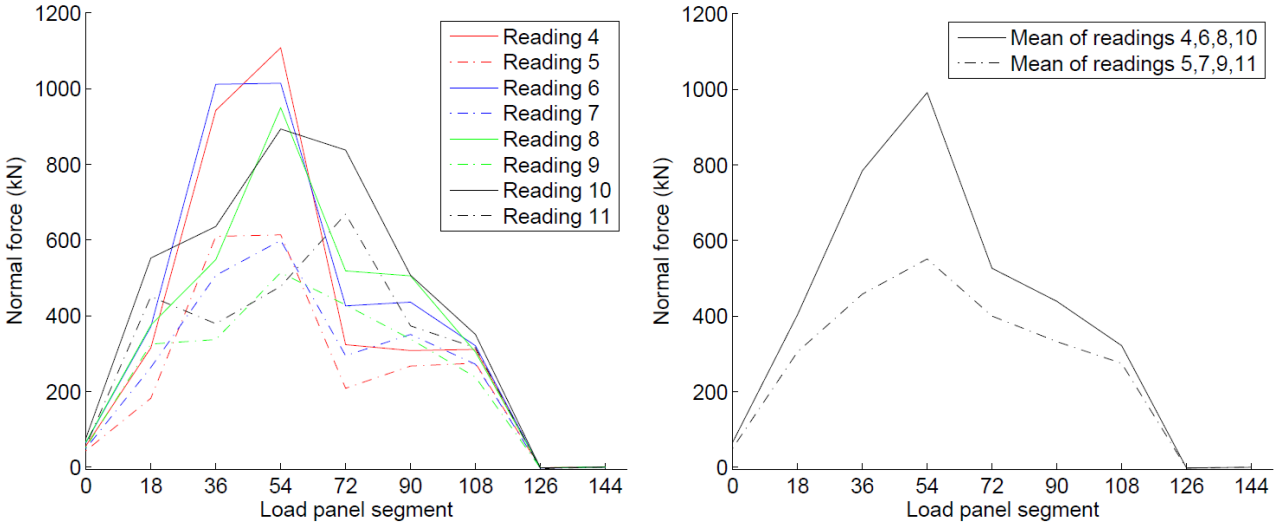

(a) (b)

Figure 3.13 (a) Comparison of force maxima and minima. (b) Mean of maxima and mean of minima.

Earlier in this chapter it was pointed out how the loading rate was low in the two panels P36 and P54 before the vibrations were initiated. After reading 4, one can observe that the slopes in the force panel time history are significantly steeper that it was between reading 1 and 3. Between reading 5 to 6, the average loading rate for P54 and P36 is 1090kN/s.

3.5 Numerical modelling of the 30031225 FLC-event

This section presents the first of two numerical simulations of the 30031225 FLC-event. In this first simulation, the ice characteristics are tuned in order to achieve a global load that resembles the load calculated from full-scale measurements. Calculations of input values for the analysis are first given, before the actual results are presented.

3.5.1 Modal analysis

Eigenfrequencies of the structure has been reported in several publications, with quite varying values. Tugboat pull tests in open water have shown first eigenfrequency at 3.5Hz while reports from measurements of IIV indicate first eigenfrequency at 2.0-2.9Hz (Popko, 2014). Fig. 3.14 shows the

first three modeshapes of the beam element model. For comparison, results from a modal analysis on a more refined finite element model (Popko, 2014) are presented in Fig. 3.15. As Fig. 3.14 indicates, deformation in the soil-structure interaction has a substantial contribution to the mode shapes.

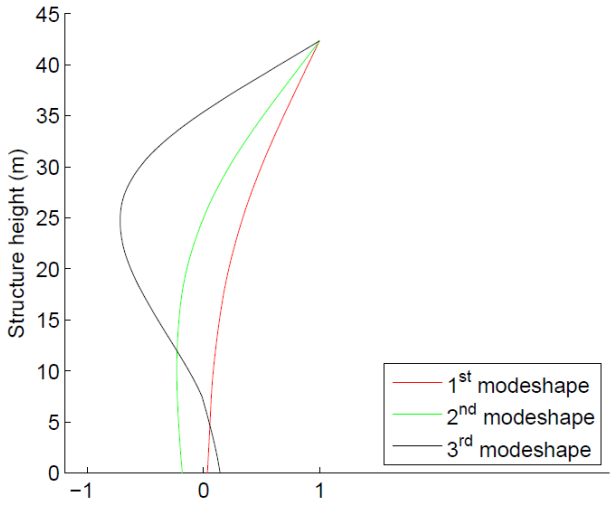

Figure 3.14 Beam element model modeshapes.

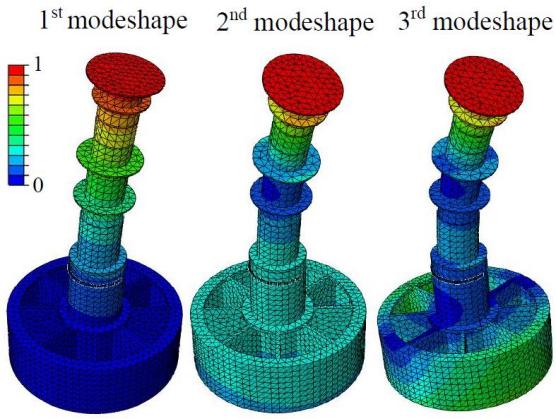

Figure 3.15 Shell element model modeshapes.

The modeshapes in Fig. 3.15 are illustrated by both deformations and a contour plot. A contour plot shows the magnitude of a value by assigning a specific color. The color scale applied in this contour plot is shown in the upper left corner of Fig. 3.15. It must be verified that the modeshapes from the beam element model and the shell element model are the same, but that requires some interpretation of the contour plot. The following observations in the contour plot characterize the shape of the eigenmodes for the shell element model:

1st modeshape:

- the dark blue color on the entire caisson means that there is no translation or rotation present in this position
- the displacement gradually increases along the height of the structure

2nd modeshape:

- the caisson is light blue, indicating a translation
- slightly darker color on the bottom of the caisson indicate a minor rotation
-the dark color above the lower balcony, at approximately 25m height, shows that the mode has no amplitude in that point

3rd modeshape:

- green and dark blue color on the caisson indicate a rotation

- dark blue color above lower balcony indicate a second point of zero amplitude (the placement of this point deviates some from 3rd modeshape in beam element model)

The eigenfrequencies from the beam element model and the shell element model, given in Table 3.1, are similar for the first two modes, but deviates for the third mode.

	1st mode	**2nd mode**	**3rd mode**
Beam element model	2.79Hz	4.23Hz	10.40Hz
Shell element mode	2.83Hz	4.17Hz	5.62Hz

Table 3.1. Natural frequencies of beam and shell element models.

Based on the modeshapes and eigenfrequencies one can conclude that for the two modal analyses, the 1st and 2nd modeshapes are similar. For the 3rd mode there is a difference.

3.5.2 Determination of ice stiffness properties

To be able to simulate the FLC-event in the most accurate manner, the ice properties in the finite element model should replicate those present during the real life event. Force measurements, together with an estimation of the structure's displacement, have been utilized to estimate the stiffness of the ice during the elastic load build up prior to failure.

The displacement signal has been found by integrating the acceleration signal twice. The accelerometers used during the measurements were located at 16.5m and 37.1m above sea bottom. To find the response in the waterline, the ratios between the response at sea level and at the point of the accelerometers had to be found. It was assumed that the response consisted primarily of the fundamental mode, something the displacement auto spectrum confirms. Results from the modal analysis gave the ratios presented in Table 3.2.

Reference position	**Desired position**	**Response ratio 1st mode**
37.1m	14.15m	0.1639
16.5m	14.15m	0.8090

Table 3.2 Response ratios 1st mode of beam element model.

Because there were two acceleration signals at hand, two displacement signals for the structure were established at 14.15m. The signals were similar in amplitude, and in phase. This confirms that the modal analysis gave reasonable results. In the end, the displacement based on measurement from the accelerometer placed at 16.5m was used, because it was the one located closest to the ice.

An effective ice stiffness K_{eff} has been calculated for each load buildup during the first nine cycles of the event, using Eq. (3.1). The average stiffness from these nine load buildups was then calculated to be 5.352E+07N/m. This stiffness has been employed in the numerical modelling of the event.

$$K_{eff} = \frac{\Delta F_G}{\Delta \delta} \tag{3.1}$$

where $\Delta F_G = F_{G,2} - F_{G,1}$, $\Delta \delta = \Delta t v_{ice} - \Delta u$, $\Delta u = u_2 - u_1$ and $\Delta t = t_2 - t_1$.

Time of the loading cycles are given in Fig. 3.16(a). Ice stiffness for each cycle is presented in Fig. 3.17.

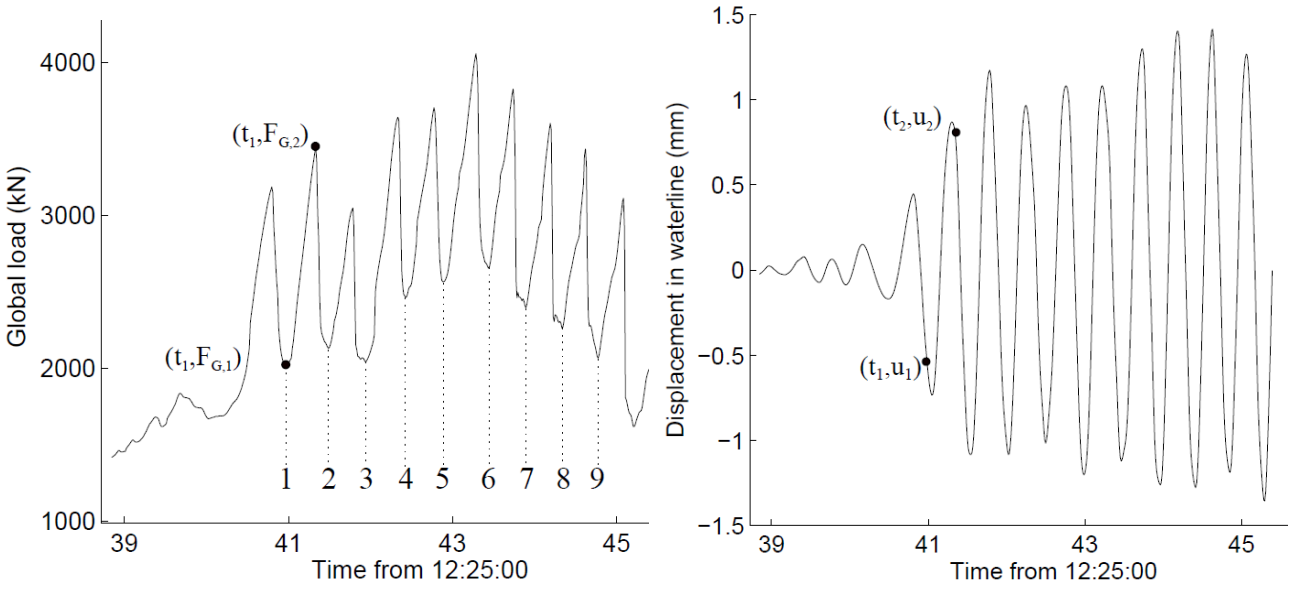

(a) (b)

Figure 3.16 (a) Global ice load and starting point of each cycle. (b) Structure displacement.

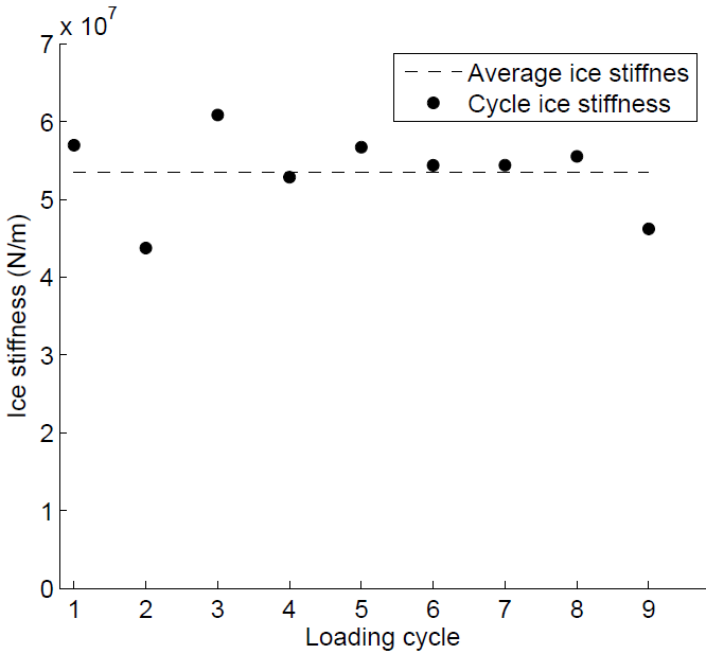

Figure 3.17 Calculated ice stiffness.

For simplicity, the ice stiffness is in the numerical analysis modelled as linearly elastic. It should be noted that the deformations in the ice during the load build up are not entirely elastic. Creep, micro-cracking and minor fractures are all non-conservative processes that soften the behavior of the ice. The real life elastic stiffness of the ice is therefore higher than what has been estimated in this calculation. However, the measured forces that work on the structure are real, and an average stiffness based on these should give reasonable results, even when it is linearized. A principle sketch of the difference between true elastic stiffness and average stiffness is illustrated in Fig. 3.18.

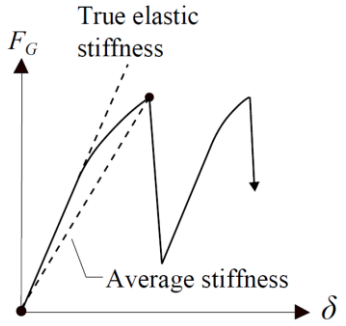

Figure 3.18 Linearized average stiffness.

3.5.3 Estimation of damping

Damping ratio of the first mode has been calculated by the half power method. A damping ratio of 3.7% was achieved. Fig. 3.19 shows the application of the half power method. Damping of the second mode was assumed to be equal to the first mode. Rayleigh damping coefficient was calculated based on these two damping ratios.

$$\zeta_1 = \frac{f_b^2 - f_a^2}{4 f_r^2} = \frac{2.260^2 - 2.090^2}{4 \cdot 2.233^2} = 0.037$$

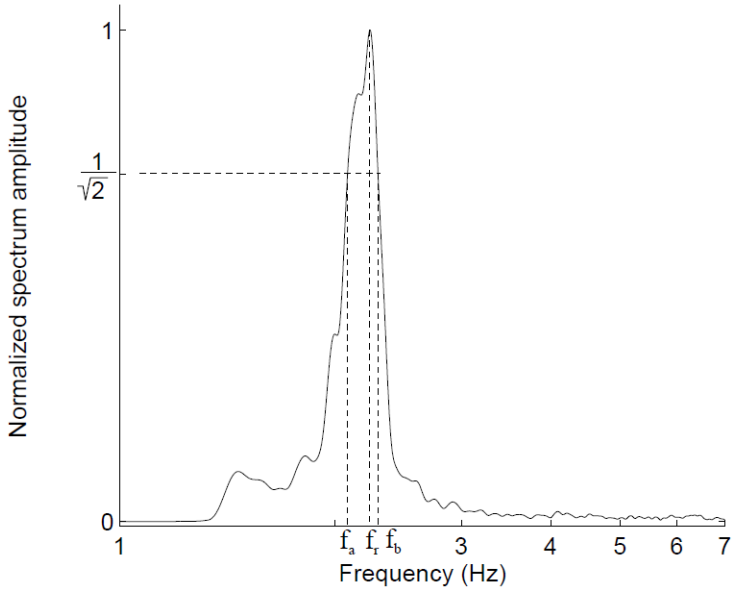

Figure 3.19 Estimation of damping.

3.5.4 Comparison of loads

The global load acting in the FE model was tuned to replicate the measured load in the full scale event. As Fig. 3.20 illustrates, the modeled load has a stable maximum level, while the magnitude of the maxima in the measured load varies. However, the objective of the analysis is the dynamic behavior of the structure. Hence, the frequency and the amplitude of the fluctuations are of greater influence than the average magnitude. Because the ice stiffness was determined, the modeled crushing length dictated the frequency of the load. A crushing length of 0.03m gave the desired crushing frequency.

Load measurements indicated that the ice failure was synchronized in the full-scale event. In the FE model all contact points are calculated separately, and therefore behaves independent of each other. To achieve synchronized failure, all contact points were designed to fail if the ice crushing capacity was exceeded in one or more contact points. This resulted in synchronized failure in all contact nodes.

While the measured load has slightly rounded change-overs at the local minima, the modeled load has a completely sharp transfer from force descend to load build up. For the inclination rate during load build up and the crushing frequency to be able to maintain the same for the two loads, the drop in load during crushing has to be slightly larger for the modeled load than the measured load.

In the plots where full-scale and finite element values are compared, the time axis shows the time for the finite element analysis. Time equal zero in the finite element analysis corresponds to approximately12:25:39.8 in the full-scale event.

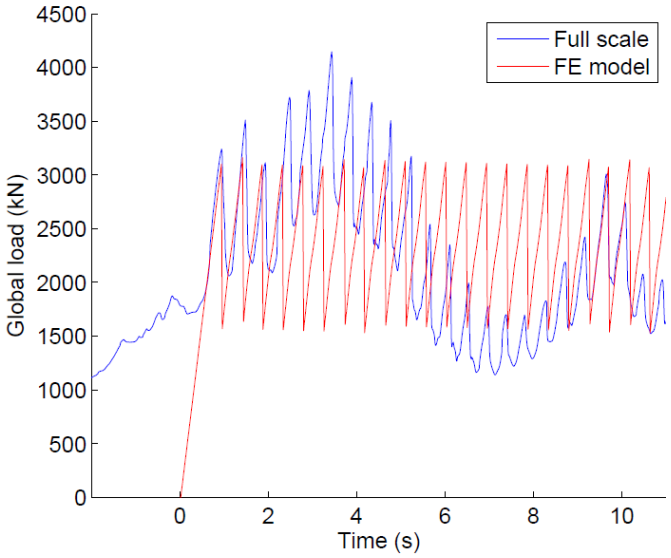

Figure 3.20 Global load.

Fig. 3.21 and Fig. 3.22 show the modeled and measured compressive forces acting on the load panels. Due to symmetry, the calculated forces on some of the load panels are equal.

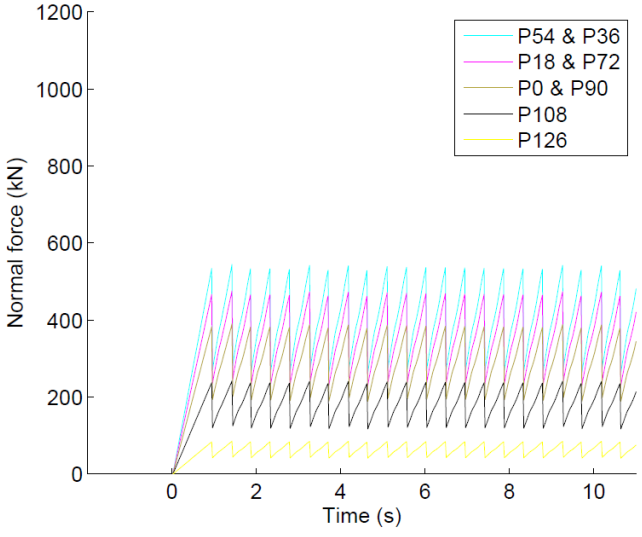

Figure 3.21 Force panels FE model.

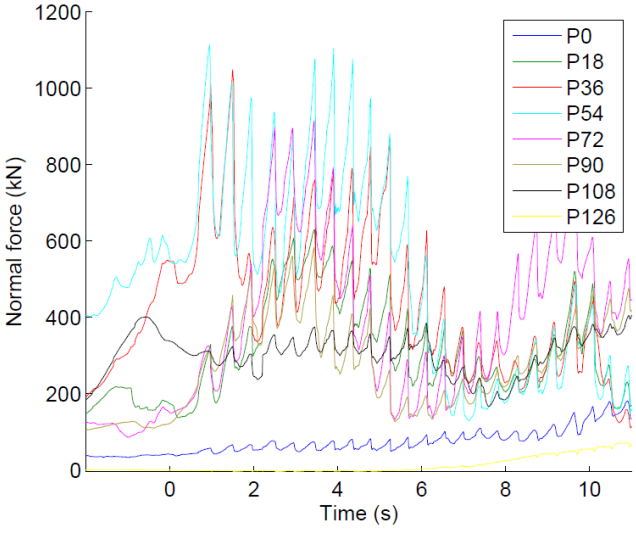

Figure 3.22 Force panels full-scale.

3.5.5 Comparison of structural response

Fig. 3.23 shows the accelerations at 16.5m height. Both signals show amplitudes in the range from -1.4m/s^2 to 1m/s^2. The peaks of negative acceleration are greater than the positive ones due to the sudden drops in both loads. On the displacement plots in Fig. 3.24, one can see that the response at

16.5m height in the FE model is lower than what is estimated from full-scale acceleration measurements. Note that low frequent content is lost when integrating the acceleration signal to establish the displacement. The presented full-scale displacement signal does therefore not include the quasistatic component

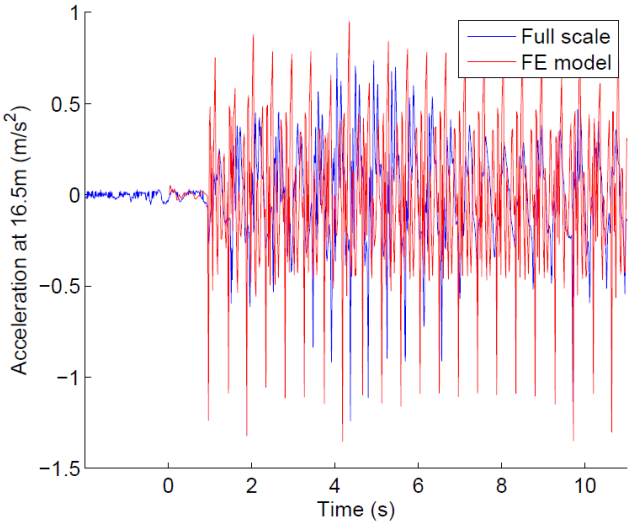

Figure 3.23 Accelerations at 16.5m.

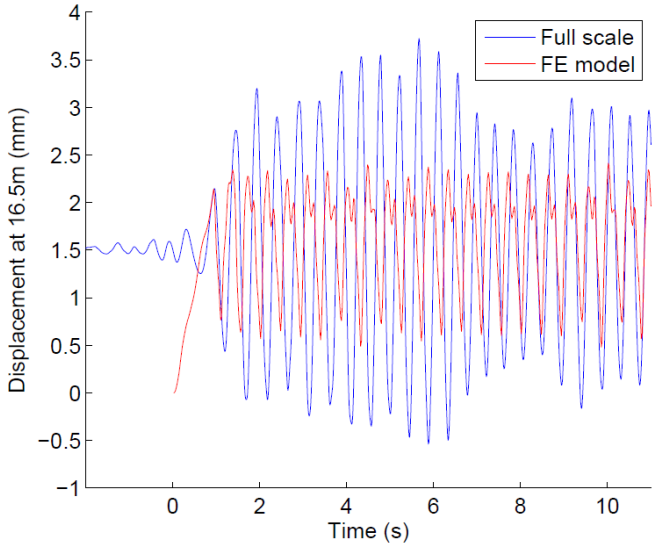

Figure 3.24 Displacements at 16.5m.

Admittedly the accuracy of a displacement signal established from integrating an acceleration signal should not be fully trusted. Nevertheless, there is a plausible explanation to why the displacements from the FE model are lower than the dispacemets from full-scale measurements. The frequency of the first eigenmode in the FE model was calculated to 2.79Hz. The frequency of the load and response was about 2.17Hz. While the full-scale displacement signal is fully sinusoidal and consists of a single frequency, the signal from the FE model indicates that there are two frequencies being exited. In Fig. 3.25 one can see how the displacement auto spectrum of the two signals verifies that there is a substantial energy at 2.167Hz and 4.333Hz in the displacement signal from the FE model. This indicates that an oscillation is excited at two times the loading frequency. When the loading excites vibrations at several frequencies, it means that the vibrations are not fully resonant, and the amplitudes are hence reduced. Increasing the loading frequency to a level closer to the first natural frequency of 2.79Hz would have given a more resonant response and increased the displacement amplitudes in the FE model.

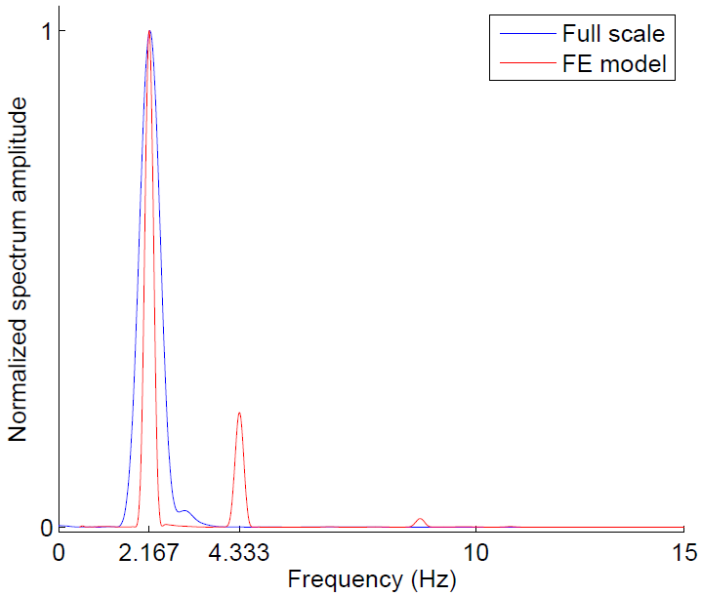

Figure 3.25 Normalized displacement auto spectrum.

3.5.6 Evaluation of stress in ice sheet

The stress and stress rates have been calculated by established expressions from theory of elasticity. In order to generate a global load similar to what was measured during the event, the crushing capacity of the ice had to be tuned. Eqs. (3.2), (3.3) and (3.4) shows the formulae that were employed in the calculations. A reduction factor of $\varphi = 0.24$ has been included to the equation for crushing capacity, proposed Määttänen (1998). The calculation of stress rate was tuned accordingly with a factor of $1/\varphi$ to account for the lowered crushing capacity. Fig. 3.26(a) shows the stress rates at the center of the interaction area, from the finite element analysis (FEA). In this area, the stress rates varied between 0.22 and 0.45MPa/s at. Based on the stress rates, one can by Fig. 3.26(b) tell that crushing capacity between 0.67 and 0.72MPa prevailed in front of the structure, during the finite element analysis.

$$\sigma_C(\dot{\sigma},\theta) = \sigma_C(\dot{\sigma})\cos(\theta) \tag{3.2}$$

$$\sigma_C(\dot{\sigma}) = \begin{cases} \varphi(2.00 + 7.80\dot{\sigma} - 18.57\dot{\sigma}^2 + 13.00\dot{\sigma}^3 - 2.91\dot{\sigma}^4)MPa & \text{for } \dot{\sigma} < 1.3\dfrac{MPa}{s} \\ \varphi MPa & \text{for } \dot{\sigma} \geq 1.3\dfrac{MPa}{s} \end{cases} \tag{3.3}$$

$$\dot{\sigma} = \frac{1}{\varphi}(v_{ice} - \dot{u})\cos^2(\theta)\frac{8\sigma(\dot{\sigma})}{\pi 1m} \tag{3.4}$$

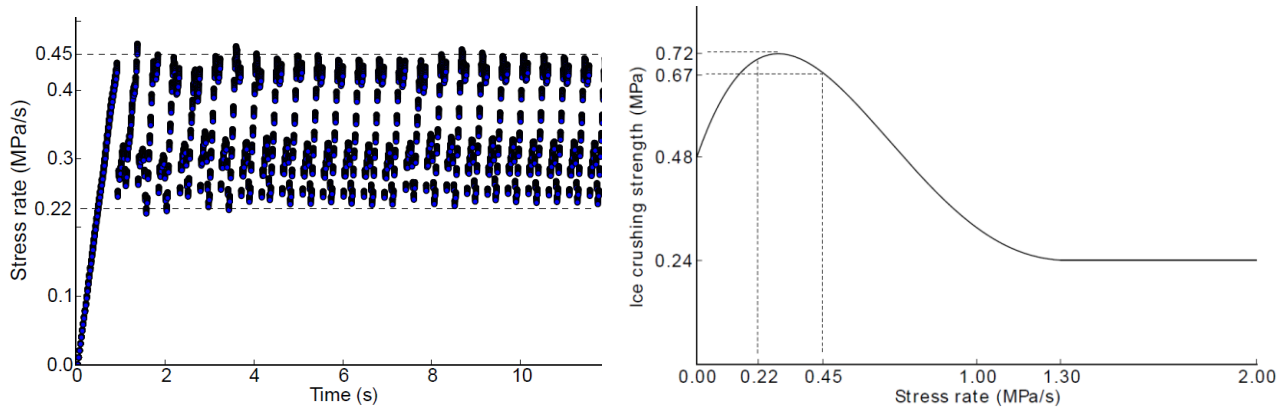

(a) (b)

Figure 3.26 (a) Stress rates in the center of interaction area, during FEA. (b) Prevailing ice crushing strength in the center of interaction area, during FEA.

3.5.7 Comparison of force distribution over interaction area

To evaluate the accuracy of the formulas employed for calculating stresses over the structure, the force distribution should be evaluated. Force distributions from the FE model has therefore been compared against the full-scale measurements. The formulae for stress calculations are based on the assumption that the compressive stress takes on a cosine distribution. Figs. 3.27(a) and (b) shows that the calculated panel forces from the FE model also have a cosine like distribution. The distribution of the measured force varies with the load level. When the global load is high, as in reading 1 and 2, the measured force distribution is concentrated to the center of the interaction area. In reading 3, where the measured global load is low, the distribution resembles something more like a cosine distribution.

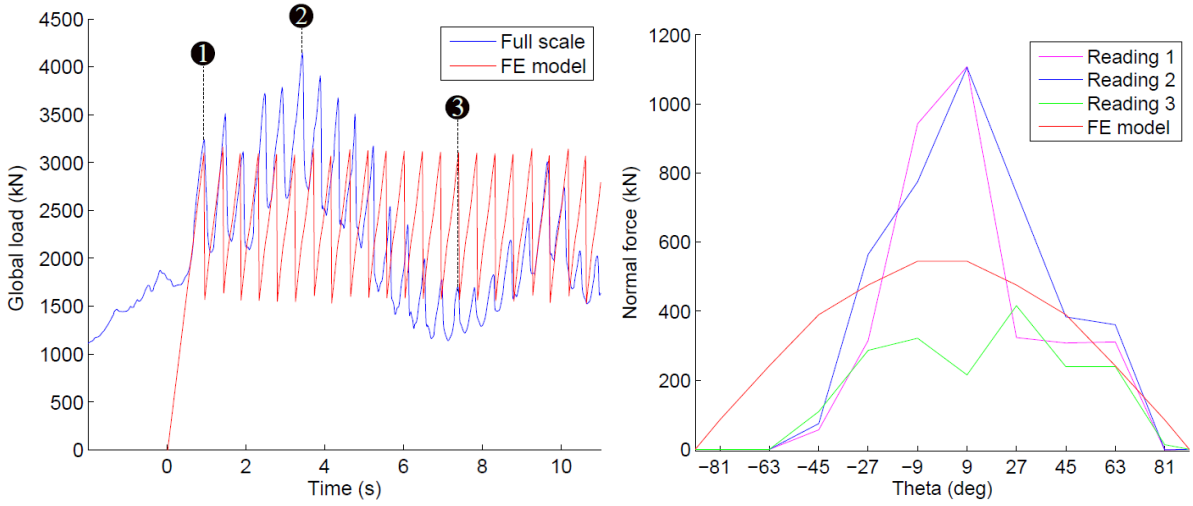

(a) (b)

Figure 3.27(a) Time of force readings. (b) Force distributions.

3.6 Numerical modelling of self-exiting vibrations

This section presents results from the second numerical simulation. First, the motivation for performing a second analysis is discussed. Then, the adaptions made for achieving self-excitation are given. Finally, results of the analysis are presented. The results from the analysis are compared with the full-scale measurements from the 30031225 FLC-event. This is done because it makes it possible to evaluate what the full-scale response looks like compared to a response that we know is due to negative damping effects.

3.6.1 Motivation for analysis

It was desirable to examine if the finite element model was able to simulate self-exciting vibrations. The results from the first simulation of the 30031225 FLC-event did not seem to be influenced by any negative damping effects, giving rise to self-excitation. Stress rate scatter plot in Fig. 3.26(a) illustrates how the stress rate operated between 0.22 and 0.45 MPa/s, which is primarily on the borderline between the ductile and the transitional domain. It is commonly believed that the stress rate operates in the transitional domain during lock-in (Yue et al., 2009). Stress rates in the transitional domain are necessary for the negative damping effect characteristic for self-exciting vibrations to be present (Blenkarn, 1970, Määttänen, 1978). In addition, the crushing process itself has to be included in the numerical integration of dynamic response. The way that the previous analysis was configured, the time between ice failure and the beginning of load build-up in the following cycle was covered in one time step. The crushing process was therefore lost. Performing a new analysis, where the crushing process is accommodated, has been attempted. The crushing process is implemented by setting the crushing length very short. During the load drop in each cycle, the modeled ice fails several times in a row. In these consecutive failures, the relative velocity increases because the structure is piercing through the ice. By representing this crushing process over several time steps, instead of including the entire ice fracture in one increment, negative damping effects has the possibility of influencing structural response.

3.6.2 Adaption of calculations

By tuning the crushing capacity, stress rate, damping and crushing length, a response indicating self-excitation was achieved. It has to be emphasized that the stress rate calculation in this analysis has been tuned to maximize negative damping effects. The applied formulae, given in Eqs. (3.5) and (3.6) are therefore not based on an analytical approach. A configuration that favored initiation of self-excited vibrations further was achieved by reducing the modal damping to $\zeta_1 = 2.0\%$ and $\zeta_2 = 2.2\%$. Rayleigh damping coefficient was calculated based on these damping ratios.

$$\sigma_C(\dot{\sigma}) = \begin{cases} 0.3(2.00 + 7.80\dot{\sigma} - 18.57\dot{\sigma}^2 - 13.00\dot{\sigma}^3 + 2.91\dot{\sigma}^4)MPa & \text{for } \dot{\sigma} < 1.3MPa \\ 0.3MPa & \text{for } \dot{\sigma} \geq 1.3MPa \end{cases} \tag{3.5}$$

$$\dot{\sigma} = 8(v_{ice} - 2\dot{r})\cos^2(\theta)\frac{8\sigma_C(\dot{\sigma})}{\pi 1m} \tag{3.6}$$

3.6.3 Result of analysis

In this analysis, the equations for stress rate were tuned to achieve stress rates that operated in the transitional domain. In Fig. 3.28(a) the resulting stress rates for each time increment in the analysis is presented. The stress rates presented are recorded for the contact node in the middle of the interaction area, where $\theta = 0$. It can be seen that the stress rates varied between 0.2 and 0.95MPa/s. The corresponding ice crushing stress is given in 3.28(b).

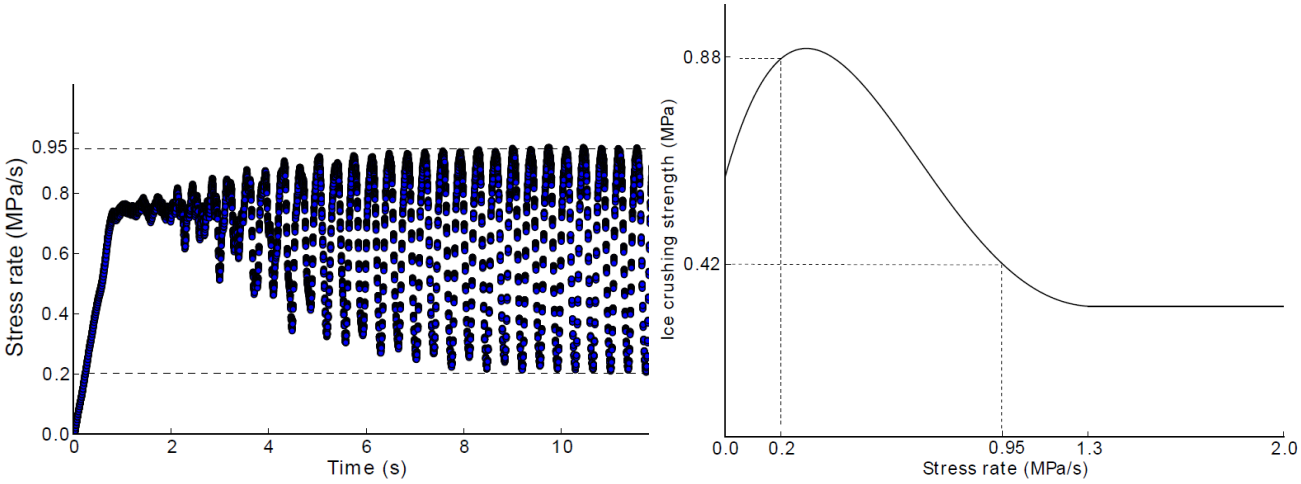

(a) (b)

Figure 3.28 (a) Stress rates in the center of interaction area, during FEA. (b) Prevailing ice crushing strength in the center of interaction area, during FEA.

The global load from the analysis, shown in Fig. 3.29, has almost no fluctuations to begin with, but together with increasing structural response, the fluctuations in load also increase.

Additional results from the analysis are presented in Figs. 3.30, 3.31 and 3.32. It is interesting to see how the displacement plot is entirely sinusoidal. The displacement auto spectrum shows how the vibrations only consist of a single frequency of 2.74Hz. This is very close to the first eigenfrequency at 2.79Hz, and a proof of the crushing locking in at the natural frequency of the structure. The saw tooth like load signal in the FE model confirms that failure in the ice was synchronized. In this analysis the contact nodes were not modeled to automatically fail simultaneously, so this means that crushing in all contact nodes self-synchronized after a few cycles of oscillations.

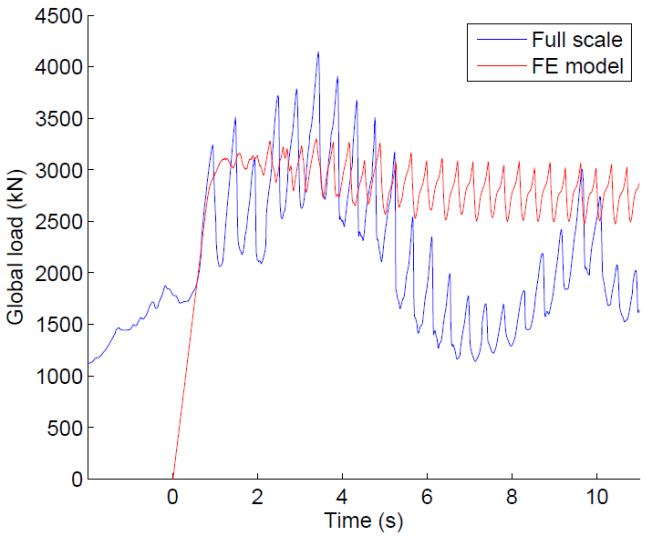

Figure 3.29 Global load.

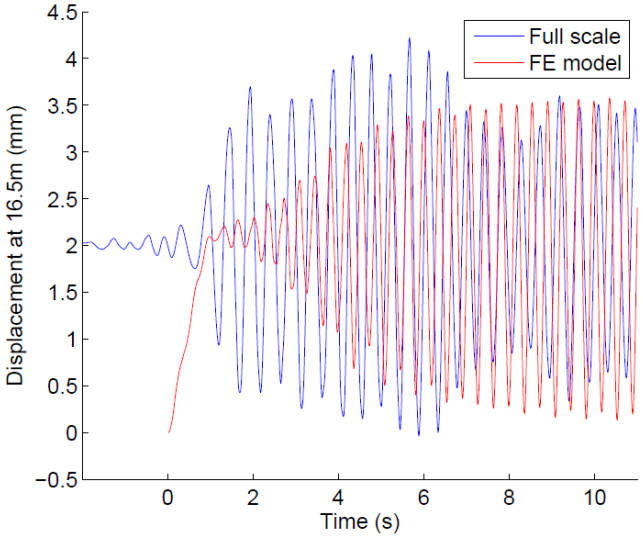

Figure 3.30 Displacement.

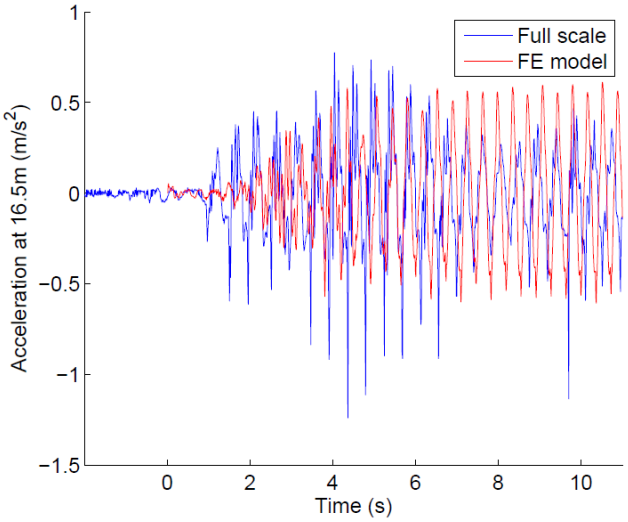

Figure 3.31 Acceleration signal.

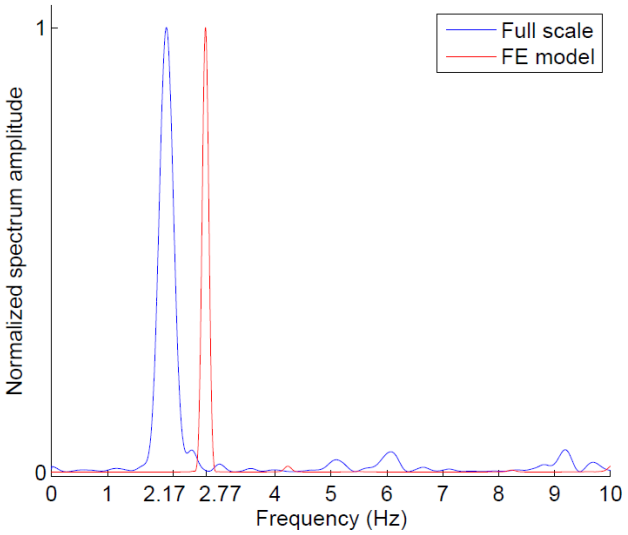

Figure 3.32 Normalized acceleration auto spectrum.

4 Discussion

It has been shown that the vibrations at Norströmsgrund 12:25 the 30th of March 2003 carry the characteristics of FLC. The relation between global load, displacements and relative velocity during the fluctuations was documented. Full-scale measurements showed that the loading and the displacements were in phase, and that the relative velocity increased rapidly after each failure of the ice. The FLC-event was simulated by two different finite element analyses. The first analysis implemented properties of the ice by analytically established expressions. In the second analysis, the equations for describing behavior of the ice were tuned to achieve vibrations due to negative damping effects.

The frequency content of the measured contact force is similar to the frequency content of the displacements, which is logical, since the ice edge and the structure are in contact and deflects together. During the lock-in event, the ice fails for each cycle of the structure's oscillations. This results in a sinusoidal steady state response, rather than a saw tooth like response. Steady state response is typical for FLC (ISO, 2010).

Even though the displacement plot shows a sinusoidal signal, the acceleration auto spectrum and the force auto spectrum indicate that higher frequencies at 4.4Hz and 6.6Hz are present in the vibrations. This can either be a superharmonic oscillation of the first mode, at two and three times the eigenfrequency, or it can be higher order modes being excited. Frequencies at multiples of the fundamental frequency have earlier been observed in force measurement on a jacket platform in the Bohai sea (Duan et al., 2002).

Synchronization of ice failure over the interaction area has been discussed in many publications regarding FLC, e.g. (Bjerkås et al., 2013, Bjerkås, 2006, Sodhi, 2001, Sodhi and Haehnel, 2003, Määttänen, 1998, Kärnä, 1992). Simultaneous failure in the contact zones will give higher load peaks on the structure. Both full-scale and model indentation tests have shown that the total ice force is lower during continuous crushing where the ice failure is non-simultaneous, than during FLC where the contact forces tends to be synchronized. This fits well with measurements from the event, which shows how the global load is highest under synchronized failure during frequency lock-in.

The failure of the ice prior to the event, resulting in a circumferential crack in front of the structure, resembles what Kärnä and Jochmann describes as a one hinge bending failure (2003). Video recordings showed that ice rubble had piled up in front of the lighthouse prior to the bending failure. It seems plausible that the weight of the rubble may have deflected the ice sheet downwards. In that case, the deformation would lead to eccentricity in the in applied in-plane force on the ice sheet. Weight of the rubble combined with eccentric load would then together cause the ice bending failure.

During the interval 12:25:30 to 12:25:39, there was contact between the ice and the centered panel P54. Given the ice velocity of 0.065m/s, the ice moved about 0.6m in 9 seconds. Due to the large relative movement, the ice must have failed several times over this period. In spite of this large relative movement between the ice and the structure, the contact force only shows minor variations. It is remarkable how the ice force increases gradually for such a long period, without any major decreases indicating ice failure.

During the nine seconds, from 12:25:30 to 12:25:39, the force increased from 86 to 614kN in panel P54. Moments later, at 12:25:40.8, we can see that the force in panel P54 reached 1100kN. This indicates that the capacity of the ice on panel P54 almost doubled in a short period of time. Increase in ice strength due to increased strain rate, when the structure velocity is higher, may explain some of this. However, integrating the acceleration signal shows that the structural velocity is very small compared to the ice velocity at 12:25:40.8. Hence, the change in strain rate due to increasing structural response is minor.

A different explanation to the increase in capacity can be the increasing confinement as contact is made for a larger sector of the structure. Simultaneous to the sudden increase in load at the mid panels, P36 and P54, there is an increase in load on the surrounding panels P18, P72 and P90. This indicates that the ice edge has gained contact with a larger part of the structure. Increased lateral confining pressure to each side may contribute to a higher capacity in the middle of the contact surface. According to Kärnä et al. (1999) the highest global loads occurs under confined conditions.

During force measurements the possibility of deficiencies in the measuring apparatus cannot be ruled out. For instance dynamic behavior of the load panel itself can disturb the recorded force.

The estimated relative velocity fluctuates between approximately 0.045m/s and 0.085m/s. These are small variations, compared to what others have found. According to Kärnä and Turunen (1990), full-scale measurements on slender channel markers in the Baltic sea, showed that during lock-in, the maximum structural velocity is equal to or higher than the ice velocity. This would indicate relative velocity equal to zero or even negative during each cycle.

Small fluctuations in relative velocity give small variations in stress rate during each loading cycle. This means that either the negative damping effect is very sensitive to changes in stress rate, or that the negative damping effect is not so decisive for frequency-lock in during the event.

Measurements show that the force distribution over the structure varies during each cycle and develops during the vibration event. Earlier it has been mentioned how a cosine force distribution over the contact area is proposed for ice structure interactions (Blenkarn, 1970, Määttänen, 1978).

Figure 4.1 shows force distributions for every 0.2 seconds during the first 20 seconds of the event. As one can see in the figure, individually the force distributions from Norströmsgrund deviate from a cosine shape. However, the force distributions are very uneven and inconsistent. Prescribing a certain load distribution is therefore a severe generalization. However, compared to the average load distribution, the cosine distribution is not so far off. It is when exceptionally high panel forces occur in the mid panels, that the cosine distribution is most wrong.

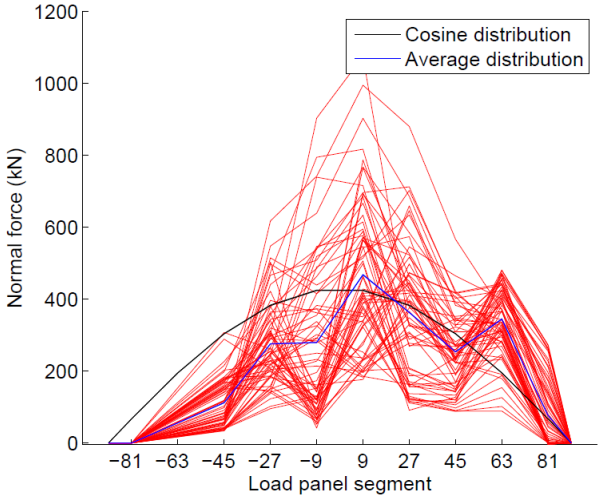

Figure 4.1 Full-scale force distributions compared to a cosine distribution.

Results from the first finite element analysis show that the model is able to reproduce structural response with fair accuracy. Because the stiffness of the ice and crushing length is predefined, the outline of the global load is more or less determined, and independent of the structural response. Even though the ice crushing strength is calculated as a function of the stress rate, the ice seems to fail at the same load level in the first failure as in the proceeding cycles. This indicates that the structure velocity has a minor influence on what force level the ice fails at. Comparing the structure velocity with the relative velocity, verifies that the variations in structure velocity are small. Because the loading pattern is close to predefined, the response is more similar to forced vibrations than self-exciting vibrations.

For the ice to fail without the global load reaching a too high level, the crushing capacity of the ice had to be set low. The rate dependent crushing capacity in the first analysis varied between 0.48 and 0.72MPa directly in front of the structure. 0.72MPa is a low compressive stress for ice to fail at, but in the finite element model, the stress distribution is unnaturally even. In real life, the stress in the interaction area will be concentrated in stress hot spots. During crushing, stresses are also known to be highest in the middle of the ice thickness (Kärnä et al., 1999). Because the stress in the finite

element model is more evenly distributed than in real life, the finite element model does not give a correct presentation of stresses present in the ice sheet during FLC.

Assuming that the modal analysis is correct, the first eigenfrequency of the structure is at about 2.8Hz. When analyzing the Pre event interval in Fig. 3.2(b), a frequency of 2.7Hz was dominating. During the FLC-event, the fluctuations attained a lower frequency of 2.2Hz. For some reason the frequency of the ice induced vibrations are reduced when the crushing mode changes from intermittent crushing to FLC. Added mass from the ice sheet can possibly explain this decrease in frequency. By an iterative approach it has been tested, how large mass that has to merge with the structure, for the first eigenfrequency of the FE model to decrease from 2.79 to 2.20Hz. In the calculations it is assumed that a point mass is added to the node in the waterline. To reduce the first eigenfrequency sufficiently, a mass of $4 \cdot 10^6 \text{kg}$ is required. This corresponds to an ice area of 75m by 75m with thickness 0.7m. For comparison, an area of 75m by 75m equals 127 times the area of the lighthouse's waterline cross section. In real life, the ice sheet is not in rigid body motion, but under elastic deformation, so only the ice in the contact zone will move as much as the structure. Deformations will gradually decrease further away from the structure. It does, however, seem plausible that added mass from the ice could affect the natural frequency of the structure in a significant manner.

Resonant response occurs when the frequency of a dynamic load is close to a natural frequency of the system. The displacement signal from the first FE simulation did not indicate that the loading created a response that was truly resonant. This could have been expected when the two first natural frequencies were at 2.79Hz and 4.23Hz and the loading at 2.17Hz.

Most ice-structure interaction models that have previously been presented treat the structural behavior by means of equations of motion for either a single or multi degree of freedom system. However the various models differ in the representation of contact force. Contact force representing either forced vibrations (Matlock et al., 1969, Sodhi, 1988) or self-exited vibrations (Määttänen, 1978, Määttänen, 1998, Blenkarn, 1970) have been the most common methods used in theoretical interaction models proposed. Forced vibrations imply that the nature of the loading is fixed, and that the structure will respond according to load. For a self-exiting system, the loading is not pre-determined but dependent on the structural response in the waterline. Self-excited ice induced vibrations are associated with negative damping effects due to rate dependency in ice crushing strength. The two analyses that have been presented in this work show that it is possible to achieve approximately the same dynamic response from a predefined load and a load from self-excitation. However, the loading during self-excitation attained the natural frequency of the structure by itself.

With the second analysis it was proven that the finite element program presented is able to represent increasing dynamic response due to negative damping effects. If the phenomenon of FLC should be denoted as self-exciting has been a matter of much discussion within the field of IIV. According to Sodhi (1988) ice induced vibration do not comply to the definition of self-exciting vibrations, because the exciting force is not eliminated if the structure is prevented from moving. However, the result from the numerical modelling shows that the loading amplitudes increased together with increasing structural response. This means that at least the fluctuation in force would be removed if the system was being held still. In the numerical model it is possible to remove nearly all fluctuation in force because the crushing length is set to be very short. In real life the ice has a larger crushing length, which would lead to fluctuations in contact force even if the structure is held still.

A weakness in the FE model is that the structural response is affected by changes in time increment length. When the ice reaches its capacity and is modeled to fail, the contact force is reduced from one time step to the next. The shorter the time step is, the more abrupt the drop in load gets. Abrupt drops in load lead to negative peaks in the acceleration signal. It should be looked more into how time steps affect the response.

The damping properties have been calculated, but the accuracy that can be expected from the applied half power method is not great. The method is intended to be applied on the frequency response function of a single degree of freedom system, so using it on the response auto spectrum which was done here, will reduce the accuracy. During resonant vibrations, the magnitude of the amplitudes is governed by the level of damping, and for the rise of self-exciting vibrations, damping definitely plays a decisive role. More emphasis should therefore be put into determining structural damping in further analyses.

5 Conclusion

The vibrations occurring at 12:25 the 30th of March 2003 on the Norströmsgrund lighthouse has been evaluated. Based on the following observations it was confirmed that the vibrations were of frequency lock-in type:

- The frequency of the crushing adapted to the frequency of the structure's waterline displacement
- The response reached a steady state
- The displacement signal was sinusoidal
- The crushing was synchronized over the interaction area

It was observed that prior to the FLC-event a circumferential crack in the ice was approaching the lighthouse. The ice in front of the crack was weakened. As a result of the crack the global force on the lighthouse was low before it started to increase when the structure gained contact with intact ice. Soon after, the vibrations initiated.

From full-scale measurements, the relation between variation in force and variation in structural response was established. It was confirmed that during the FLC-event:

- The fluctuations in global load and displacements were in phase
- The relative velocity decreased during load build up and increased when the ice failed
- The frequency of the vibrations of the lighthouse was reduced from 2.7Hz during intermittent crushing to 2.2Hz during frequency lock-in crushing.

The horizontal force distribution has been evaluated for several points of time during the onset of the vibrations. Force measurements showed that:

- The fluctuations in force were most prominent in center of the interaction area
- For the average load, a cosine distribution is a reasonable assumption

A finite element program was developed to recreate the FLC-event. It was demonstrated that the finite element program is able to recreate the structural response of the Norströmsgrund lighthouse with fair accuracy. It was also tested if dynamic response due to negative damping effects from the rate dependency of ice crushing strength could be modelled with the finite element program. It became clear that the crushing process had to be modelled over several time steps for the negative damping to affect the structural response. By tuning the equation for stress rate, vibrations due to negative damping effects was achieved.

References

BJERKÅS, M. 2006. *Ice Actions on Offshore Structures.* Ph.D., NTNU.

BJERKÅS, M. 2014. *RE: Personal Communication.*

BJERKÅS, M., MEESE, A. & ALSOS, H. 2013. Ice Induced Vibration - Observations of a Full Scale Lock-in Event. *Proceeding of the twenty-third Offshore and Polar Engineering***,** 1272 - 1279.

BJÖRK, B. 1981. Ice-induced Vibrations of Fixed Offhore Structures Part 2: Experience with Baltic Lighthouses. *Marine Structures and Ships in Ice.*

BLENKARN, K. A. 1970. Measurement and Analysis of Ice Forces on Cook Inlet Structures. *Second Annual Offshore Technology Conference*.

CHOPRA, A. K. 2011. *Dynamics of Structures,* Prentice-Hall.

COOK, R. D., MALKUS, D. S., PLESHA, M. E. & WITT, R. J. 2002. *Concept and application of finite element analysis,* Wiley.

COWPER, G. R. 1966. Shear Coefficient in Timoshenko Beam Theory. *Journal of Applied Mechanics***,** 335-346.

DEN HARTOG, J. P. 1956. *Mechanical vibrations,* New York, McGraw-Hill.

DUAN, Z., OU, J. & SPENCER, B. F. INVESTIGATION OF ICE FORCES ON JACKET PLATFORM STRUCTURES: IN-SITU MEASURED DATA ON JZ20-2-1 PLATFORM IN THE CHINA BOHAI SEA. 15th ASCE Engineering Mechanics Conference, 2002 Columbia University, New York.

FREDERKING, R. & BARKER, A. 2001. Friction of Sea Ice on Various Construction Materials. *In:* CANADA, N. R. C. O. (ed.).

GAVIN, H. P. 2014. Structural Element Stiffness and Mass Matrices. Department of Civil and Environmental Engineering: Duke University.

GRAVESEN, H., SØRENSEN, S. L., VØLUND, P., BARKER, A. & TIMCO, G. W. 2005. Ice loading on Danish wind turbines: Part 2. Analyses of dynamic model test results. *Cold Regions Science and Technology,* 41**,** 25-47.

HE, J. & FU, Z.-F. 2001. *Modal Analysis,* Boston, Butterworth-Heinemann.

HUANG, G. & LIU, P. 2009. A Dynamic Model for Ice-Induced Vibration of Structures. *Journal of Offshore Mechanics and Arctic Engineering,* 131.

ISO 2010. ISO19906:2010 Petroleum and natural gas industries – Arctic offshore structures. International Organization of Standarization.

JOCHMANN, P. 2003. Full Scale Measurements at Lighthouse Norströmsgrund – Winter 2001. *STRICE REPORT.* Hamburg: Hamburgische Schiffbau-Versuchsanstalt GmbH.

KÄRNÄ, T. A procedure for dynamic soil-structure-ice interaction. International Offshore and Polar Engineering, 1992 San Fransisco. 765-771.

KÄRNÄ, T. & JOCHMANN, P. FIELD OBSERVATIONS ON ICE FAILURE MODES. 17th International Conference on Port and Ocean Engineering under Arctic Conditions, 2003 Trondheim.

KÄRNÄ, T., KAMESAKI, K. & TSUKUDA, H. 1999. A numerical model for dynamic ice-structure interaction. *Computers and Structures,* 72.

KÄRNÄ, T. & TURUNEN, R. 1989. DYNAMIC RESPONSE OF NARROW STRUCTURES TO ICE CRUSHING. *Cold Regions Science and Technology***,** 173-187.

KÄRNÄ, T. & TURUNEN, R. A STRAIGHTFORWARD TECHNIQUE FOR ANALYSING STRUCTURAL RESPONSE TO DYNAMIC ICE ACTION. International Conference of Offshore Mechanics and Arctic Engineering, 1990 Houston, USA.

KÄRNÄ, T. & YAN, Q. 2003. A Spectral Model for Dynamic Ice Actions. *STRICE.*

LANGEN, I. & SIGBJÖRNSSON, R. 1979. *Dynamisk analyse av konstruksjoner,* Tapir.

MATLOCK, H., DAWKINS, W. P. & PANAK, J. J. 1969. A Model for the Prediction of Ice-Structure Interaction. *First Annual Offshore Technology Conference,* 1.

MICHEL, B. & TOUSSAINT, N. 1977. Mechanisms and theory of indentation of ice plates. *Journal of glaciology,* 19**,** 285-300.

MÄÄTTÄNEN, M. 1978. *On conditions for the rise of self-excited ice induced autonomous oscillations in slender marine pile structures.* Ph.D., University of Oulo.

MÄÄTTÄNEN, M. Numerical model for ice-induced vibration load lock-in and synchronization. 14th International Symposium on Ice, 1998 New York. 923-930.

PALMER, A. C., GOODMAN, D. J., ASHBY, M. F. & PONTER, A. R. S. 1983. FRACTURE AND ITS ROLE IN DETERMINING ICE FORCES ON OFFSHORE STRUCTURES. *Annals of Glaciology,* 4**,** 216-221.

PEYTON, H. R. 1968. *Sea Ice Strength.* Doctor, University of Alaska.

POPKO, W. COMPARISON OF FULL-SCALE AND NUMERICAL MODEL DYNAMIC RESPONSES OF NORSTRÖMSGRUND LIGHTHOUSE (under review). International Conference on Ocean, Offshore and Arctic Engineering, 2014 San Fransisco.

RÖNNQUIST, A. 2005. *Pedestrian induced lateral vibrations of slender footbridges.* Ph.D., Norwegian University of Science and Technology.

SANDERSON, T. J. O. 1988. *Ice mechanics: risks to offshore structures,* Graham & Trotman.

SODHI, D. S. 1988. Ice Induced vibration of Structures. *IAHR Ice Symposium,* Vol. 3**,** pp. 625-657.

SODHI, D. S. 1991. Energy exchanges during indention tests in fresh-water ice. *Annals of Glaciology,* 15**,** 247 - 253.

SODHI, D. S. 2001. Crushing failure during ice-structure interaction. *Engineering Fracture Mechanics,* 68**,** 1889-1921.

SODHI, D. S. & HAEHNEL, R. B. 2003. Crushing Ice Forces on Structures. *Journal of cold regions engineering,* 153.

STRANNEBY, D. 2001. *Digital Signal Processing*, Butterworth-Heinemann.

STRØMMEN, E. 2010. *Theory of Bridge Aerodynamics*, Springer.

SUKHORUKOV, S. & MARCHENKO, A. 2014. Geometrical stick–slip between ice and steel. *Cold Regions Science and Technology***,** 8-19.

TIMCO, G. W. & WEEKS, W. F. 2009. A review of the engineering properies of ice. *Cold Regions Science and Technology,* 60**,** 107-129.

TIMOSHENKO, S. P. & GOODIER, J. N. 1951. *Theory of elasticity,* New York, McGraw-Hill.

WESSELS, E., JOCHMANN, P. & HOFFMANN, L. FIRST RESULTS OF ICE FORCE MEASUREMENTS WITH TIP-PANELS AT NORSTRÖMSGRUND LIGHTHOUSE. Port and Ocean Engineering Under Arctic Conditions, 1989 Luleå. 1428-1439.

YUE, Q., GOU, F. & KÄRNÄ, T. 2009. Dynamic ice forces of slender vertical structures due to ice crushing. *Cold Regions Science and Technology,* 56**,** 77-83.

APPENDICES

Contents

Appendix A

Iterative Newmark routine

Iterative Newmark scheme as presented by Langen and Sigbjörnsson (1979)

Symbols

$\{\ddot{\mathbf{u}}\}$ = Acceleration vector

$\{\dot{\mathbf{u}}\}$ = Velocity vector

$\{\mathbf{u}\}$ = Displacement vector

$[\mathbf{K}_{IK}]$ = Stiffness matrix

$[\mathbf{C}_{IK}]$ = Damping matrix

$\{\mathbf{Q}_K\}$ = Load vector

A) *Initial calculations*

1 Establish mass matrix $[\mathbf{M}]$

2 Establish initial response vectors $\{\mathbf{u}\}$, $\{\dot{\mathbf{u}}\}$ and $\{\ddot{\mathbf{u}}\}$

3 Specify integration parameter γ and β

4 Calculate the following constants

$a_1 = \frac{\gamma}{\beta \Delta t}$	$a_5 = \frac{\gamma}{\beta}$
$a_2 = \frac{1}{\beta \Delta t^2}$	$a_6 = \Delta t(\frac{\gamma}{2\beta} - 1)$
$a_3 = \frac{1}{\beta \Delta t}$	$a_7 = \frac{\gamma}{\beta} - 1$
$a_4 = (\frac{1}{2\beta} - 1)$	$a_8 = (1-\gamma)\Delta t$
	$a_9 = \gamma \Delta t$

5 Calculate mass contribution to effective stiffness $[\hat{\mathbf{M}}] = a_2[\mathbf{M}]$

B) *For every time step:*

1 If a new incremental stiffness or damping matrix is established, calculate $[\hat{\mathbf{K}}_K]$

$$[\hat{\mathbf{K}}_K] = [\mathbf{K}_{IK}] + a_1[\mathbf{C}_{IK}] + [\hat{\mathbf{M}}]$$

2 Calculate effective load vector

$$\{\Delta\hat{\mathbf{Q}}_K\} = \{\mathbf{Q}_{K+1}\} + [\mathbf{C}_{IK}]\{\mathbf{b}_K\} + [\mathbf{M}]\{\mathbf{a}_K\} - \{\mathbf{F}_K^D\} - \{\mathbf{F}_K^S\}$$

where $\{\mathbf{a}_K\} = a_3\{\dot{\mathbf{u}}_K\} + a_4\{\ddot{\mathbf{u}}_K\}$

$$\{\mathbf{b}_K\} = a_5\{\dot{\mathbf{u}}_K\} + a_5\{\ddot{\mathbf{u}}_K\}$$

$$\{\mathbf{F}_K^D\} = [\mathbf{C}_{IK}]\{\dot{\mathbf{u}}_K\}$$

$$\{\mathbf{F}_K^S\} = [\mathbf{K}_{IK}]\{\mathbf{u}_K\}$$

3 Solve for displacement increment

$$\{\Delta\mathbf{r}_K\} = [\hat{\mathbf{K}}_K]^{-1}\{\Delta\hat{\mathbf{Q}}_K\}$$

4 If necessary, solve for dynamic equilibrium

a) Set $\{{}^0\Delta\mathbf{u}_K\} = \{\Delta\mathbf{u}_K\}$, $i = 0$

$$\{\mathbf{d}_K\} = a_7\{\dot{\mathbf{u}}_K\} + a_6\{\ddot{\mathbf{u}}_K\}$$

b) Calculate approximations to accelerations, velocities and displacements

$$\{{}^{i-1}\ddot{\mathbf{u}}_{K+1}\} = a_2\{{}^{i-1}\Delta\mathbf{u}_{K+1}\} - \{\mathbf{a}_K\}$$

$$\{{}^{i-1}\dot{\mathbf{u}}_{K+1}\} = a_1\{{}^{i-1}\Delta\mathbf{u}_{K+1}\} - \{\mathbf{d}_K\}$$

$$\{{}^{i-1}\mathbf{u}_{K+1}\} = \{\mathbf{u}_K\} + \{{}^{i-1}\Delta\mathbf{u}_{K+1}\}$$

c) Calculate effective residual forces

$$\{{}^{i-1}\Delta\mathbf{F}_K\} = \{\mathbf{Q}_{K+1}\} - [\mathbf{M}]\{{}^{i-1}\ddot{\mathbf{u}}_{K+1}\} - \{{}^{i-1}\mathbf{F}_{K+1}^D\} - \{{}^{i-1}\mathbf{F}_{K+1}^S\}$$

d) Solve for correction of displacement increment

$$\{{}^i\Delta\} = [\hat{\mathbf{K}}_K]^{-1}\{{}^{i-1}\Delta\mathbf{F}_K\}$$

e) Calculate new displacement increment

$$\{{}^i\Delta\mathbf{u}_K\} = \{{}^{i-1}\Delta\mathbf{u}_K\} + \{{}^i\Delta\}$$

f) Convergence test

$$\left\| {}^i\Delta \right\|_{M2} < tol.$$

If the convergence test is passed, go to 5.

If not and $i < MAXIT$, set *i=i+1 and go to b)*

If $i \geq$ *MAXIT stop analysis.*

5 Calculate acceleration, velocity and displacement at t_{K+1}

$$\{\ddot{\mathbf{u}}_{K+1}\} = a_2\{\Delta\mathbf{u}_K\} - \{\mathbf{a}_K\}$$

$$\{\dot{\mathbf{u}}_{K+1}\} = \{\dot{\mathbf{u}}_K\} + \mathrm{a}_8\{\ddot{\mathbf{u}}_K\} + \mathrm{a}_9\{\ddot{\mathbf{u}}_{K+1}\}$$

$$\{\mathbf{u}_{K+1}\} = \{\mathbf{u}_K\} + \{\Delta\mathbf{u}_{K+1}\}$$

References:

Langen, I. and R. Sigbjörnsson (1979). Dynamisk analyse av konstruksjoner, Tapir.

Appendix B

Deduction of equation for radial ice stress

Global ice force is calculated by summing normal and tangential forces for all contact nodes (Eq. (B-1)).

$$F_G = 2\sum_i F_i \cos(\theta_i) + F_i^T \sin(\theta_i) \tag{B-1}$$

where $i = 1-158$ is the contact nodes, and $F_i^T = \mu F_i$ is the tangential contact force

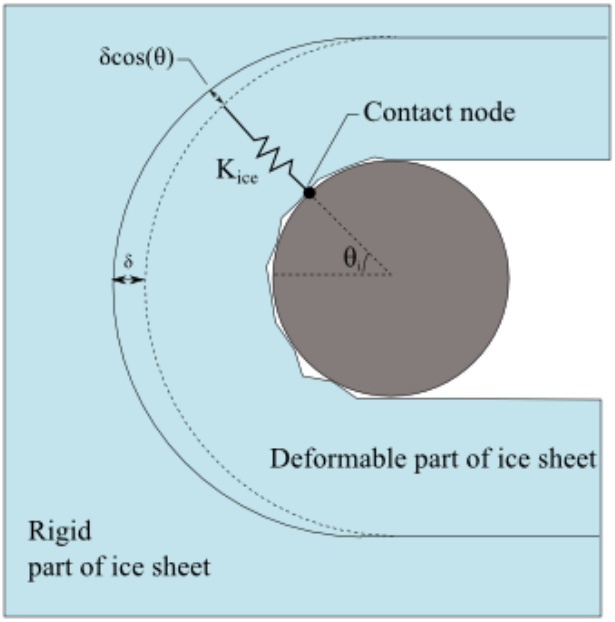

Figure B-1. Contact node, δ and K_{ice}.

Normal force acting on a contact node is given by

$$F_i = K_{ice}\delta\cos(\theta_i) \tag{B-2}$$

where δ is the deformation in the ice and K_{ice} is the stiffness of an area of ice equal to $0.01rh$ (one contact node).

Inserting for F_i in Eq. (B-2), gives the following expression for global force

$$F_G = 2\sum_i K_{ice}\delta\cos(\theta_i)\left(\cos(\theta_i) + \mu\sin(\theta_i)\right) \tag{B-3}$$

The effective stiffness of the ice is defined by the expression

$$K_{eff}\delta = F_G \tag{B-4}$$

Combining Eqs. (B-3) and (B-4) and solving for K_{ice} gives

$$K_{ice} = \frac{K_{eff}}{2\sum_i \cos(\theta_i)\left(\cos(\theta_i) + \mu \sin(\theta_i)\right)} \tag{B-5}$$

The radial stress acting over the area of one node can then be expressed as

$$\sigma_i = \frac{K_{ice}\delta\cos(\theta_i)}{0.01rh} = \frac{K_{eff}\delta\cos(\theta_i)}{0.01rh2\sum_i \cos(\theta_i)(\cos(\theta_i) + \mu\sin(\theta_i))} \tag{B-6}$$

On a continuous format Eq. (B-6) can be expressed as

$$\sigma(\theta) = \frac{K_{eff}\delta\cos(\theta)}{2rh\int_0^{\frac{\pi}{2}} \cos^2(\theta) + \mu\cos(\theta)\sin(\theta)\,\mathrm{d}\theta} \tag{B-7}$$

Appendix C

Load module flow chart

Flowchart of loadmod.py. Points 1 to 5 are calculated for each contact node. Point 6 sums up contribution for each contact node.

Symbols

t^N = time
u^N = structure displacement
$\dot{u}^N$ = structure velocity
x^N = parameter reducing ice deformation after crushing
u_{ice}^N = ice movement
v_{ice} = ice velocity
v_{rel}^N = relative velocity between ice and structure
δ^N = ice deformation
σ_C^N = ice crushing capacity
σ^N = radial ice stress
$\dot{\sigma}^N$ = ice stress rate
φ = scaling factor
F_G = global ice load
c = crushing length

0 Input from previous time step is imported:

$$t^N,\ u^N,\ \dot{u}^N,\ x^N$$

1 Initial values are determined:

$$u_{ice}^N = t^N v_{ice},\ v_{rel}^N = v_{ice} - \dot{u}^N,\ \ \delta^N = u_{ice}^N - x^N - u^N$$

2 Stress rate is calculated based on stress in previous time step:

$$\dot{\sigma}^N = \frac{1}{\varphi}(v_{ice} - \dot{u}^N)\cos^2(\theta)\frac{8\sigma^{N-1}}{\pi 1m}$$

3 Ice crushing capacity is calculated based on stress rate:

$$\sigma_C^N(\dot{\sigma}^N)=\begin{cases}\varphi(2.00+7.80\dot{\sigma}^N-18.57(\dot{\sigma}^N)^2+13.00(\dot{\sigma}^N)^3-2.91(\dot{\sigma}^N)^4)MPa & \text{for } \dot{\sigma}<1.3\dfrac{MPa}{s}\\ \varphi MPa & \text{for } \dot{\sigma}\geq 1.3\dfrac{MPa}{s}\end{cases}$$

4 Calculate ice stress (predictor step):

$$\sigma^N(\theta)=\frac{K_{eff}\delta^N\cos(\theta)}{2rh\int_0^{\frac{\pi}{2}}\cos^2(\theta)+\mu\cos(\theta)\sin(\theta)\,\mathrm{d}\theta}$$

5 Check if stress exceeds crushing capacity:

If $\sigma^N<\sigma_C^N$ go to 6

If $\sigma^N\geq\sigma_C^N$, set $x^N=u_{ice}^N-u^N-(\delta^N-\mathrm{c})$ and then recalculate (corrector step)

$$\delta^N=u_{ice}^N-x^N-u^N$$

$$\dot{\sigma}^N=\frac{1}{\varphi}(v_{ice}-\dot{u}^N)\cos^2(\theta)\frac{8\sigma^{N-1}}{\pi 1m}$$

$$\sigma_C^N(\dot{\sigma}^N)=\begin{cases}\varphi(2.00+7.80\dot{\sigma}^N-18.57(\dot{\sigma}^N)^2-13.00(\dot{\sigma}^N)^3+2.91(\dot{\sigma}^N)^4)MPa & \text{for } \dot{\sigma}<1.3\dfrac{MPa}{s}\\ \varphi MPa & \text{for } \dot{\sigma}\geq 1.3\dfrac{MPa}{s}\end{cases}$$

$$\sigma^N(\theta)=\frac{K_{eff}\delta^N\cos(\theta)}{2rh\int_0^{\frac{\pi}{2}}\cos^2(\theta)+\mu\cos(\theta)\sin(\theta)\,\mathrm{d}\theta}$$

6 Calculate global force (sums up contribution from all contact nodes):

$$F_G^N=2hr\int_0^{\frac{\pi}{2}}\sigma^N(\theta)\cos(\theta)+\mu\sigma^N(\theta)\sin(\theta)d\theta$$

The global force is then used to calculate the structural response in time step *N+1*.

Appendix D

Calculation of compensating densities

Caisson:

Part	Number	Height (m)	Width (m)	Thickness (m)	Ø outer (m)	Ø inner (m)	Volume (m^3)	Density (m^3)	Mass (kg)
Bulkheads	8	5.25	7.38	0.40	-	-	124.0	2400	297562
Bottom plate	1	0.7	-	-	23.0	-	290.8	2400	697998
Top plate	1	1.50	-	1.50	23.0	7.2	562.1	2400	1349137
Outer tube	1	5.25	-	0.50	23.0	21.96	192.8	2400	462722
Inner tube	1	6.75	-	0.50	7.2	6.2	71.0	2400	170494
Sand in compartments	8	5.25	-	-	22.0	7.2	1871.7	2000	3743422
Sand in inner tube	1	6.75	-	-	6.2	-	203.8	2000	407574
Sum	-	-	-	-	-	-	-	-	**7128909**
Modeled volume	1	7.45	-	0.52	23.0	21.96	273.6	**26057**	-

Lower tube:

Part	Number	Height (m)	Width (m)	Thickness (m)	Ø outer (m)	Ø inner (m)	Volume (m^3)	Density (m^3)	Mass (kg)
Sand in tube	1	9.05	-	-	6.2	-	273.2	2000	546451
Tube	1	9.05	-	0.50	7.2	6.2	95.2	2400	228588
Top plate	1	0.30	-	-	7.2	-	12.2	2400	29315
Sum	-	-	-	-	-	-	-	-	**804354**
Modeled volume	1	9.05	-	-	7.2	6.2	95.2	**8445**	-

For the slabs in the lighthouse, the density is set to 2500kg/m^3, while the hollow sections between the slabs are given the density of 2650kg/m^3 to compensate for interior.